Glacial and hydrothermal sources of dissolved iron(II) in Southern Ocean waters surrounding Heard and McDonald Islands

Thomas M. Holmes[1,2,†], Kathrin Wuttig[1], Zanna Chase[2], Christina Schallenberg[1], Pier van der Merwe[1], Ashley T. Townsend[3], and Andrew R. Bowie[1,2]

[1]Antarctic Climate and Ecosystems Cooperative Research Centre (ACE CRC), University of Tasmania, Private Bag 80, Hobart, Tasmania 7001, Australia.

[2]Institute for Marine and Antarctic Studies (IMAS), University of Tasmania, Private Bag 129, Hobart, Tasmania, Australia.

[3]Central Science Laboratory (CSL), University of Tasmania, Private Bag 74, Hobart, TAS 7001, Australia.

Corresponding author: Thomas M. Holmes (Thomas.holmes@utas.edu.au)

†Current address: School of Oceanography, University of Washington, Box 357940, Seattle, WA 98105, USA.

Key Points:

- Remote Heard and McDonald Islands are distinct iron(II) sources in the Southern Ocean
- The main iron(II) source at Heard Island is glacial, while hydrothermal vents are the main source of iron(II) near McDonald Islands
- Results highlight complex iron cycling at a Southern Ocean biological hotspot, with implications for regional bioavailability of iron

Abstract

The Southern Ocean is the largest region in which iron limits the growth of phytoplankton. However, a phytoplankton bloom thousands of square kilometres in area forms each spring-summer in the Indian sector of the Southern Ocean, both above and to the east of the Kerguelen Plateau. The central region of the Kerguelen Plateau hosts the volcanically active islands, Heard and McDonald (HIMI), the former of which is largely covered by glaciers. The sources and processes governing supply of iron from HIMI to the region are relatively unknown. In the austral summer of 2016, the first voyage to focus on biogeochemical cycling in the HIMI region was undertaken (GEOTRACES process study GIpr05). Using iron redox measurements, we show here that each of the adjacent islands are strong sources of dissolved iron(II) (DFe(II)), though controlled by different supply mechanisms.

At Heard Island, the greatest DFe(II) concentrations (max 0.57 nmol L^{-1}) were detected north of the island. An inverse correlation of DFe(II) concentrations with salinity suggests the origin is from a sea-terminating glacier on the island. At McDonald Islands, the greatest DFe(II) concentrations (max 1.01 nmol L^{-1}) were detected east of the islands which, based on DFe(II) profiles from five targeted stations, appears likely to originate from shallow diffuse hydrothermalism. Elevated DFe(II) around HIMI may increase Fe availability for biota and indicate slower oxidation kinetics in the region, which has implications for transport of Fe away from the islands to the broader northern Kerguelen Plateau where the annual plankton bloom is strongest.

Plain language summary

Phytoplankton form the base of the aquatic food web, produce comparable atmospheric oxygen to terrestrial plants and help moderate global heating through uptake of CO_2. Thus, it is vital to know what influences phytoplankton growth in the ocean. Along with nutrients such as nitrate and phosphate, phytoplankton require iron for growth. Iron concentrations are

very low in the Southern Ocean, limiting the growth of phytoplankton. However, near the Kerguelen Plateau in the Indian sector of the Southern Ocean, a phytoplankton bloom thousands of square kilometres in area forms each spring-summer. There are two volcanically active islands in the central region of the Kerguelen Plateau – Heard and McDonald. Volcanic activity supplies iron in various forms to the ocean, yet these islands have not been studied in detail. Iron(II) is a short-lived yet preferred form of iron for phytoplankton in the ocean. Using iron(II), we show that these closely spaced islands supply iron in different ways. Underwater volcanic vents supply iron near McDonald Island, while glacial runoff supplies iron near Heard Island. Knowing these iron sources is essential for understanding what causes this large phytoplankton bloom at the Kerguelen Plateau, an important ecological hotspot and contributor for regulation of atmospheric CO_2.

1. Introduction

Iron (Fe) is a key limiting, or co-limiting, micronutrient for biological primary production (Martin et al., 1990) in as much as half of the world's oceans (Moore et al., 2009), with important implications for biogeochemical cycling and the drawdown of carbon from the atmosphere (Boyd and Ellwood, 2010). The most energetically stable form of Fe in the oxygenated ocean, Fe(III), has low solubility. The reduced form of Fe, Fe(II), is more soluble in seawater and should be kinetically more bioavailable to phytoplankton (Shaked et al., 2005). However, Fe(II) is only present as a transient species in the oxygenated ocean, generally existing in vanishingly low concentrations (picomolar or less) due to rapid (minutes to days) oxidation by oxygen (O_2) and hydrogen peroxide (H_2O_2) in surface waters (Millero et al., 1987).

Nevertheless, continuous production of Fe(II) by several processes in the ocean can lead to measurable quantities in both surface and deeper waters. In the surface ocean, concentrations of Fe(II) are increased by photochemical reduction of organic-Fe(III) complexes (Rijkenberg

et al., 2005), wet and dry atmospheric deposition (Croot and Heller, 2012), glacial melt in higher latitudes (Raiswell et al., 2018 and references therein) and biological production by processes such as viral lysis of cells and grazing (Hansard et al., 2009 and references therein). In the deeper ocean and on continental shelves, sources include benthic fluxes from anoxic and sub-oxic sediments (Lohan and Bruland, 2008), hydrothermal fluids (Holmes et al., 2017; Sedwick et al., 2015) and redox cycling induced by oxygen minimum zones (Lohan and Bruland, 2008). Thus, given the rapid loss of Fe(II) in oxygenated seawater, measurements of Fe speciation can be used as a near-field tracer of processes and sources of Fe biogeochemistry in the ocean (Holmes et al., 2017).

The oxidation kinetics of Fe(II) in seawater are complex, depending on many factors including pressure, temperature, salinity, O_2 concentration, H_2O_2 concentration and pH (Millero et al., 1987; Millero and Sotolongo, 1989; Santana-Casiano et al., 2006). At the pH of seawater, the oxidation rate of Fe(II) is heavily dependent on O_2 and H_2O_2 concentrations, with the relative influence of each species dependent on its concentration (Santana-Casiano et al., 2006). Rainwater and biological production can contribute to the H_2O_2 inventory (Croot et al., 2004). Rainwater scavenges H_2O_2 from the atmosphere (Cohan et al., 1999), increasing surface ocean concentrations through direct deposition; however, this process is more prevalent in lower latitudes (Weller and Schrems, 1993). Studies have also demonstrated biological production of H_2O_2 in the water column (Palenik and Morel, 1988) but the major source of H_2O_2 in the ocean is through photochemical reactions involving dissolved organic matter and O_2 (Croot et al., 2004). When concentrations of H_2O_2 are less than 200 nmol L^{-1}, Fe(II) is at nanomolar levels and pH is 8, O_2 becomes the most important oxidant. Therefore, it is important to consider both of these oxidants when analysing Fe(II) cycling.

The Southern Ocean (SO) is the largest region of Fe deficiency in the World's oceans (Boyd et al., 2007). However, within the Indian sector of the SO, there is an oasis of relatively Fe

rich waters overlaying the Kerguelen Plateau. At the southern part of the central Kerguelen plateau is an active volcanic hotspot, hosting two active subaerial volcanic islands, Heard and McDonald (HIMI), the former of which is largely covered by glaciers. Waters in the region are subject to an intense mixing regime, caused by strong winds, shallow bathymetry characterised by many seamounts and ridges, and the location of the plateau in the path of strong currents associated with the polar front to the north and Fawn Trough Current to the south of HIMI (Figure 1; Park et al., 2014). Fed by the Fe-rich waters formed on the plateau, a plankton bloom on the order of thousands of square kilometres forms over and downstream of the plateau each spring and summer (Blain et al., 2007). In the austral summer of 2016, the first voyage to focus on biogeochemical cycling in the HIMI region was undertaken: Heard Earth-Ocean-Biosphere Interactions (HEOBI). In the context of an interdisciplinary study centred around hydrothermalism, we measured dissolved Fe(II) (DFe(II)) and hydrogen peroxide (H_2O_2) to uncover which sources and processes were important for the distribution and oxidation kinetics of DFe(II) around HIMI, with implications for Fe bioavailability and transport of Fe to the northern plateau.

2. Methods

2.1. Study area

Sampling and shipboard analyses were carried out aboard R/V *Investigator* during the HEOBI voyage (GEOTRACES process study GIpr05) from January 8th to February 27th 2016 around Heard and McDonald Islands (HIMI) on the Kerguelen Plateau in the Indian sector of the SO. Twenty-seven stations were successfully sampled for both DFe(II) and H_2O_2 (Figure 1), with an extra four stations sampled for H_2O_2 only (not shown). The same locations were also occupied by Conductivity-Temperature-Depth rosette (CTD) casts, along with an additional 22 CTD only stations (not shown).

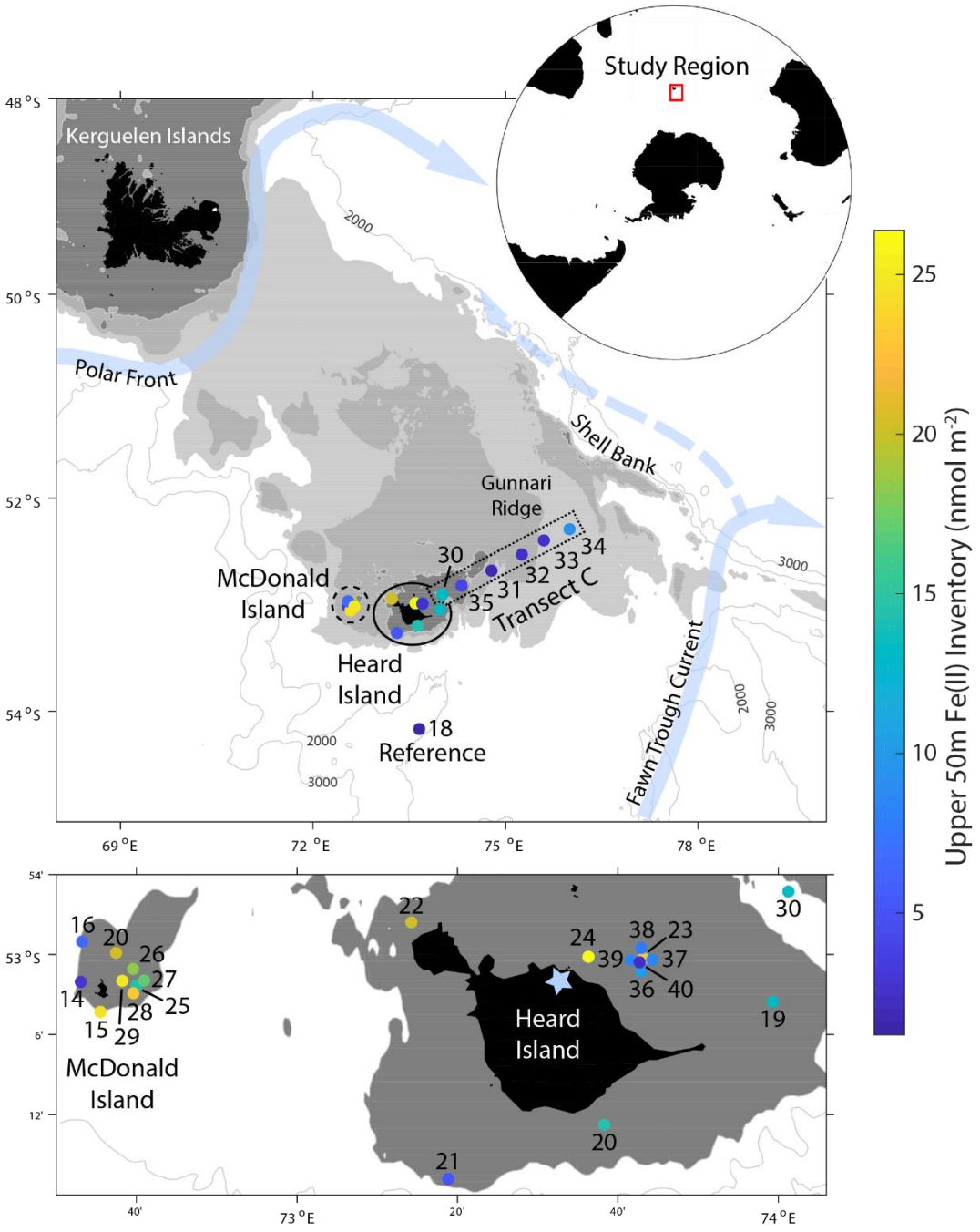

Figure 1. DFe(II) integrated inventory in the upper 50 m at each station sampled for DFe(II) during HEOBI. Concentrations indicated by colour bar. TMR station numbers and regions are annotated. Location of study region is shown in top inset. Heard and McDonald Islands are shown zoomed in bottom inset. Transect C (dotted square) follows the first 150 km of 'Transect C' from a previous voyage (Kerguelen Ocean and Plateau Compared Study: KEOPS-1; Blain et al., 2008). The reference station was located to the south of HIMI in high-nutrient, low chlorophyll (HNLC) waters. Bathymetric isobaths are shown, with seabed <200 m depth shaded dark grey, <500 m shaded lighter grey and <1000 m shaded lightest grey. Major currents are shown in light blue arrows, adapted from Park et al., (2014). Downes and Ealey marine terminating glaciers are marked by a blue star on Heard Island.

Sample stations were divided into 4 regions: Transect C, Heard Island, McDonald Islands and reference stations. Transect C was oriented in a northeast-southwest direction, with the aim of

highlighting the near shore to deep water gradient in biogeochemical tracers. Transect C extends from Heard Island across Gunnari Ridge towards Shell Bank, crossing almost perpendicular to the prevailing current, which flows northward along the plateau. This transect followed the same trajectory as the previous KEOPS-1 'C' transect in 2005 (Blain et al., 2008), though not reaching as far to the northeast as the previous transect, which extended off the plateau into waters >3500 m deep.

Sampling station locations in the HIMI region were selected based on bathymetric features (Watson et al., 2016) and acoustic flare signals detected with shipboard echosounders (Spain et al., 2019) suggesting potential hydrothermal activity (see section 3.1). Acoustic flare signals had distinct characteristics when caused by seafloor gas seepage (Spain et al., 2019). Based on these criteria, two sites were chosen for an additional five stations located in a crosshair pattern – one at McDonald Islands (stations 25 – 29) and one at Heard Island (stations 36 – 40) – in an attempt to further delineate possible hydrothermal inputs.

A reference site, (station 18) was sampled ~100 km to the south of Heard Island, located in waters more representative of HNLC conditions (max 0.81 mg m^{-3} Chl*a* in upper 200 m; Wojtasiewicz et al., 2019). Mean currents at this station were associated with the Fawn Trough Current, moving from west (open ocean) to east (plateau; Figure 1; Park et al., 2014).

2.2. Sample collection

Briefly, all water column samples were collected in 12 L Niskin bottles modified for trace metal sampling, deployed using the Australian Marine National Facility trace-metal-clean rosette (TMR) equipped with a Seabird CTD unit and attached to a Dyneema rope. Once recovered, the Niskin bottles were rapidly transferred into a trace-metal-clean containerised laboratory for sub-sampling and sample processing. All sample manipulation and analyses were conducted following GEOTRACES guidelines (Cutter et al., 2014) under ISO 5 HEPA

filtered air within the containerised clean room. Both DFe(II) and H_2O_2 samples were collected in acid-cleaned, dark brown (low-light transmittance), high-density polyethylene (Nalgene) sample bottles. Dissolved Fe(II) samples were filtered through acid-washed Pall Acropak Supor capsule filters (0.2 µm) while samples for H_2O_2 were not filtered. Samples were immediately double bagged and put directly on ice. Samples were then transported into a separate trace metal clean analytical container for immediate analysis (DFe(II) within 1 hour, H_2O_2 within 2 hours). To ensure that any oxidation of DFe(II) which occurred between subsampling and analysis was consistent, every effort was made to keep the time between subsampling and analysis as consistent as possible at each station.

2.3. Dissolved iron(II) analysis

Dissolved Fe(II) samples were analysed using flow injection - chemiluminescence analysis (FIA-CL) with in-line preconcentration onto an 8-HQ resin adapted from the method of Bowie et al., (2005, 2002) and recently described by Sedwick et al., (2015). Briefly, a 0.02 µmol L^{-1} DFe(II) stock solution was prepared before the voyage by dissolving trace metal grade ammonium iron(II) sulfate hexahydrate (Aldrich) in 0.1 µmol L^{-1} ultrapure hydrochloric acid (Seastar Baseline) solution. The stock solution was kept in darkness for the duration of the voyage. Working solutions of 200 µmol L^{-1} and 200 nmol L^{-1} concentrations were prepared daily via serial dilution with 0.1 mol L^{-1} HCl. All DFe(II) stock solutions contained sodium sulphite as a stabilising agent. Calibration standards were also prepared daily from the stock solution, in aged low-Fe seawater, buffered with 0.4 µmol L^{-1} ammonium acetate to a pH of ~6. Calibration standards covered a concentration range of 0 – 1.2 nmol L^{-1} (which was adequate for the majority of samples collected) and were analysed before each block of samples from individual stations.

The blank solution used for the DFe(II) FIA analysis consisted of low Fe seawater collected during the cruise. Triplicate blank measurements were taken both before and after each

analysis sequence. Analysis times were recorded for each sample. For instances where instrument signal drift was noted between the initial and final blank measurements, a blank value was calculated for each sample via linear interpolation.

The detection limit of the DFe(II) FIA-CL instrument was defined as the analyte concentration equivalent to three times the standard deviation of the blank peak (n=3) (Bowie et al., 2004). During the HEOBI voyage the detection limit was calculated each day and ranged from 0.02 to 0.16 nmol L^{-1} with a mean of 0.06 nmol L^{-1} (n = 17).

2.4. Dissolved hydrogen peroxide analysis

Dissolved H_2O_2 samples were analysed using a FIA-CL reagent injection method (Yuan and Shiller, 1999). Briefly, H_2O_2 catalyses the chemiluminescence of luminol in the presence of Co^{2+} at alkaline pH. H_2O_2 standards were prepared by serial dilution from a 30% stock solution (Seastar Baseline) and were determined by spectrophotometric measurements with a 10 cm Liquid Waveguide Capillary Flow Cell (LWCC, World Precision Instruments, ε = 40.9 mol L^{-1} cm^{-1}; Hwang and Dasgupta, 1985). Each seawater sample was analysed at least four times with a typical precision of 3 – 5% through the concentration range 0.5 – 75 nmol L^{-1} and a typical detection limit (3σ) of 0.6 nmol L^{-1}.

2.5. Modelling dissolved iron(II) half-lives

Shipboard pH data was unavailable during HEOBI. Therefore, using in-situ O_2, H_2O_2, salinity, temperature and depth data, expected Fe(II) half-lives over the pH range 7.1 – 8.2 (the pH range of historical observations in the region, taken from the World Ocean Database; Tanhua et al., 2013) were modelled using a method modified from Hansard et al. (2009). The overall rate of oxidation of Fe(II) is given by:

$$\frac{-dFe(II)}{dt} = k_{app,O_2}[Fe(II)][O_2] + k_{app,H_2O_2}[Fe(II)][H_2O_2] \#(1)$$

where $k_{app,O2}$ and $k_{app,H2O2}$ are the apparent rate constants (M^{-1} min^{-1}) for oxidation by O_2 and H_2O_2, respectively. When oxidants are in excess, the reaction is pseudo first-order, and is given by:

$$\frac{-dFe(II)}{dt} = (k'_{O_2} + k'_{H_2O_2})[Fe(II)]\#(2)$$

where k'_{O2} (min^{-1}) = $k_{app,O2}[O_2]$ and $k'_{[H2O2]}$ (min^{-1}) = $k_{app,h2O2}[H_2O_2]$. The overall half-life with respect to oxidation is:

$$T_{half} = 0.693(k'_{O_2} + k'_{H_2O_2})^{-1}\#(3)$$

The k'_{O2} value was calculated following Millero et al. (1987) as follows:

$$\frac{-dFe(II)}{dt} = k'_{O_2}[Fe(II)]\#(4)$$

where

$$k'_{O_2} = k[OH]^2[O_2]\#(5)$$

The rate constant k can be calculated for a given temperature and ionic strength (see equations in Millero et al., 1987). Similarly, k'_{H2O2} was calculated according to Millero and Sotolongo (1989), with some assumptions:

$$\frac{-dFe(II)}{dt} = k'_{H_2O_2}[Fe(II)]\#(6)$$

where

$$k'_{H_2O_2} = k[H_2O_2][OH^-]\#(7)$$

These calculations assume that $[H_2O_2]$>>[Fe(II)], which makes the oxidation of Fe(II) by H_2O_2 pseudo-first order.

2.6. Hydrographic data and dissolved iron data

Temperature, salinity, pressure and oxygen data were taken from Sea-Bird Electronics SBE3T, SBE4C, SBE9plus and SBE43 sensors respectively, which were mounted on the primary CTD rosette. Total dissolved iron (DFe) data, including collection and analysis methods are reported in Holmes et al., (2019).

3. Results

3.1. Dissolved Fe(II) distribution

3.1.1. Transect C

All Transect C stations were located above the plateau. The three most easterly stations (32, 33 and 34) had deep mixed layers, shoaling slightly towards the east (285, 254 and 245 m, respectively). Surface DFe(II) concentrations were low (mean upper 50 m concentrations, ≤ 0.15 nmol L^{-1}) compared to stations 30 and 23 at the western end of the transect (closer to HIMI), increasing to 0.29 and 0.44 nmol L^{-1} mean in the upper 50 m, respectively (Figure 2). A subsurface DFe(II) maximum was observed at Stations 31 – 34. Concentrations in this maximum layer decreased from 0.21 to 0.15 nmol L^{-1} between stations 31 to 34, while the depth of the layer increased from 97 to 297 m (Figure 2).

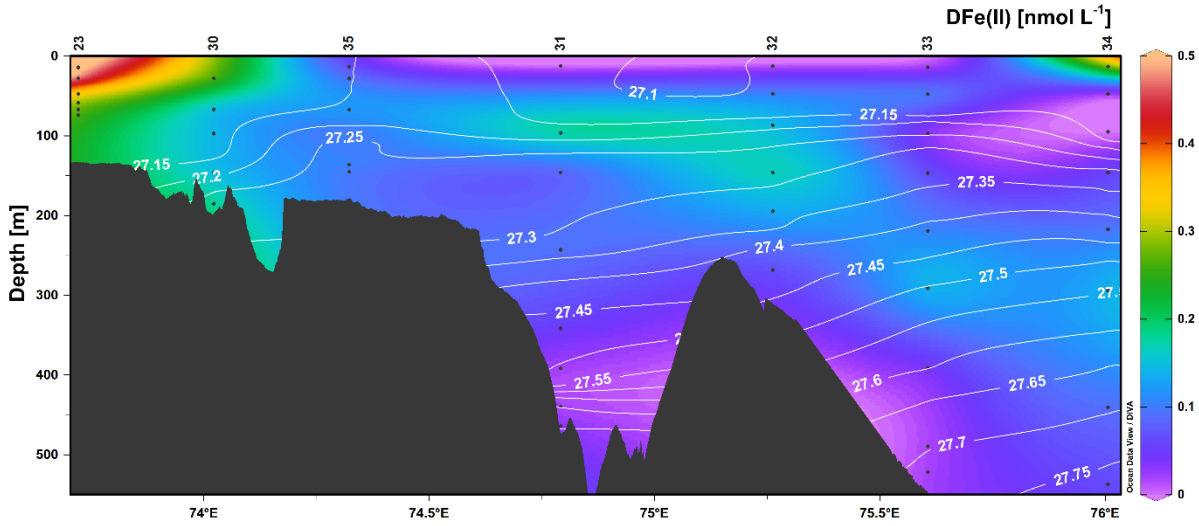

Figure 2. Transect C DFe(II) concentrations, with neutral density (γ^n; kg m^{-2}) surfaces overlaid (white lines, calculated from continuous CTD data). Black dots represent sample locations. Station numbers for TMR deployments are shown above the top axis.

3.1.2. Heard and McDonald Islands

Concentrations of DFe(II) were elevated around HIMI relative to transect and reference stations, with relatively homogeneous profiles throughout the water column (Figure 3). McDonald Islands had a significantly higher mean DFe(II) concentration (0.36 ± 0.16 nmol L^{-1}, n = 56) compared to Heard Island (0.24 ± 0.14 nmol L^{-1}, n = 57; *t*-test, $p<0.01$). At Heard Island, the maximum DFe(II) concentration (0.57 nmol L^{-1}) was located at station 24, north of the island and near Downes and Ealey marine-terminating glaciers. At McDonald Islands, the maximum DFe(II) concentration (1.01 nmol L^{-1}) was located to the east of the island. DFe(II) inventories calculated in the upper 50 m (minimum station depth at HIMI was ~48 m, measured at station 24) are shown in Figure 1, along with arrows showing general circulation features, adapted from Park et al., (2014). Stations to the south and east of Heard Island had lower DFe(II) inventories than stations to the north of Heard Island. Stations to the west of McDonald Islands had lower DFe(II) inventories than stations to the east of McDonald Islands. This distribution corresponds to higher concentrations on the shallower, plateau side of the islands.

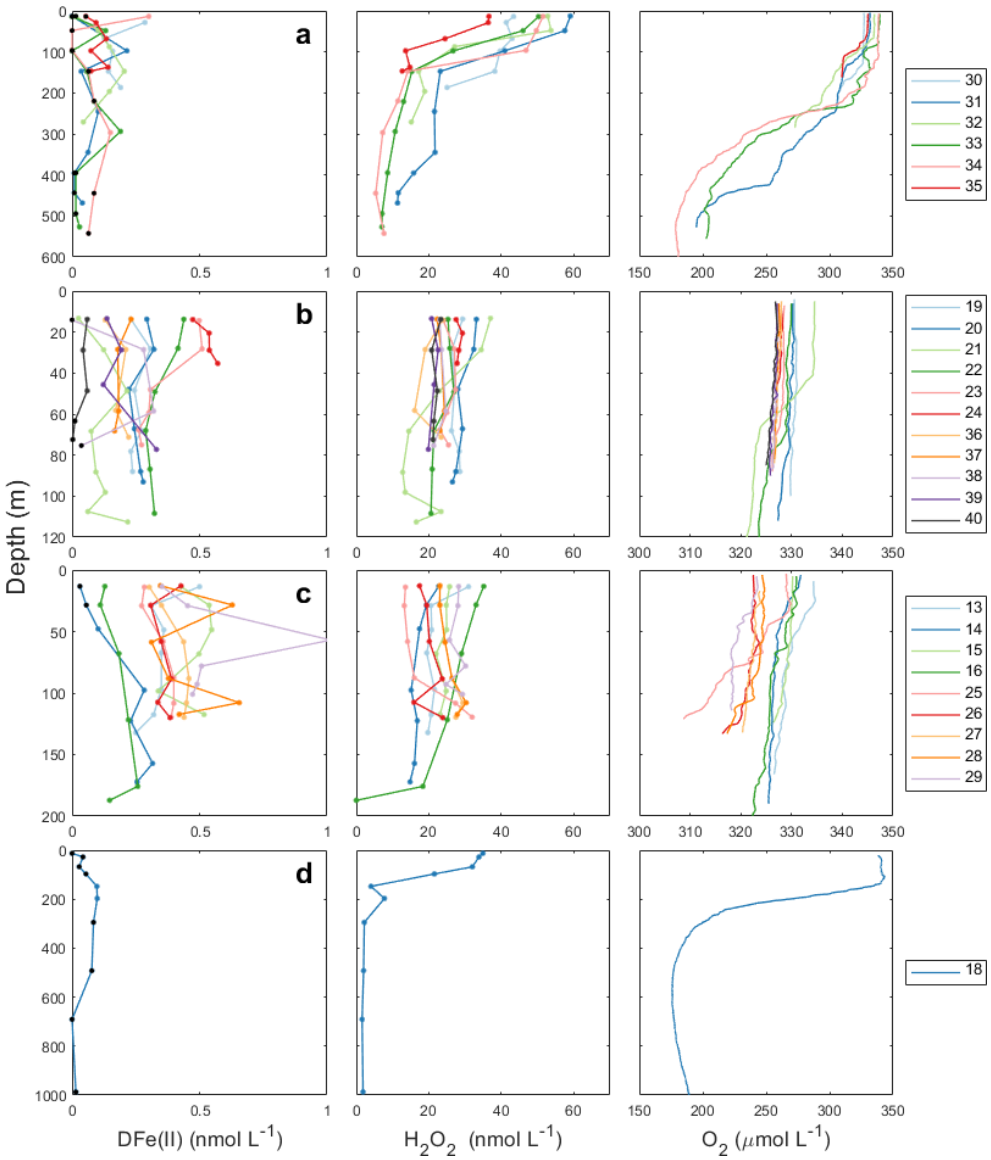

Figure 3. Profiles of DFe(II), H_2O_2 and O_2 for **a.** Transect C, **b.** Heard Island, **c.** McDonald Islands, and **d.** Reference station. Stations are colour coded and shown in legends on the right hand side of each region. Samples that were below the calculated detection limit for each station are shown in black. Note that O_2 x-axis scales vary.

3.1.3. Reference station

Surface DFe(II) concentrations were very low at reference station 18 (measured 0.03 ± 0.02 nmol L^{-1} mean in the upper 100m, n = 4, though two samples were below detection limit), increasing to a maximum (0.10 nmol L^{-1}) at 197 m before decreasing with depth (Figure 3).

3.2. Dissolved H_2O_2 distribution

3.2.1. Transect C

Greater surface concentrations of H_2O_2 were observed at stations 31 – 34 (>48 nmol L^{-1}) towards the east of transect C compared to stations 35, 30 and 23 (41.9 – 25.3 nmol L^{-1}) towards the west of the transect, with the lowest surface concentration observed closest to HIMI at station 23 (Figure 4). The distribution of H_2O_2 closely followed density layers, with concentrations at stations 31 – 34 decreasing slightly with depth, while stations 35, 30 and 23 became increasingly homogenised over the water column towards HIMI.

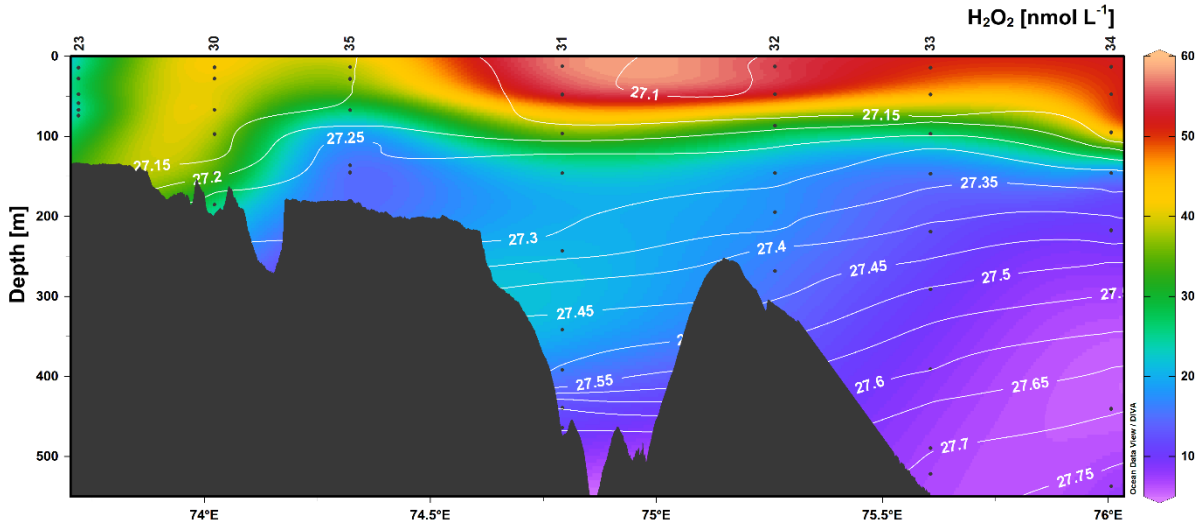

Figure 4. Transect C H_2O_2 concentrations, with neutral density (γ^n; kg m^{-2}) surfaces overlaid (white lines, calculated from continuous CTD data). Black dots represent sample locations. Station numbers for TMR deployments are shown above the top axis.

3.2.2. Heard and McDonald Islands

Surface concentrations of H_2O_2 around HIMI were highest at stations most likely affected by open ocean waters flowing along the western edge of the plateau and associated with the Fawn Trough Current: station 16, northwest of McDonald, and stations 20 and 21 south of HIMI. All other stations had homogeneous H_2O_2 profiles, with surface concentrations ranging between 13.5 – 31.0 nmol L^{-1} at McDonald Islands and 20.8 – 29.3 nmol L^{-1} at Heard Island (Figure 3).

3.2.1. Reference Station

The mean surface H_2O_2 concentration in the upper 100 m was 30.6 ± 6.1 nmol L^{-1}, n = 4. Hydrogen peroxide rapidly decreased with depth down to 200 m (the mixed layer depth) and then decreased more gradually to 1000 m (Figure 3).

3.3. Modelled DFe(II) half-lives

Within the pH range 7.1 – 8.2 (the pH range of historical observations in the region, taken from the World Ocean Database; Tanhua et al., 2013), modelled DFe(II) half-lives ranged between 30 minutes – 172 hours, decreasing with increasing pH (Figure 5).

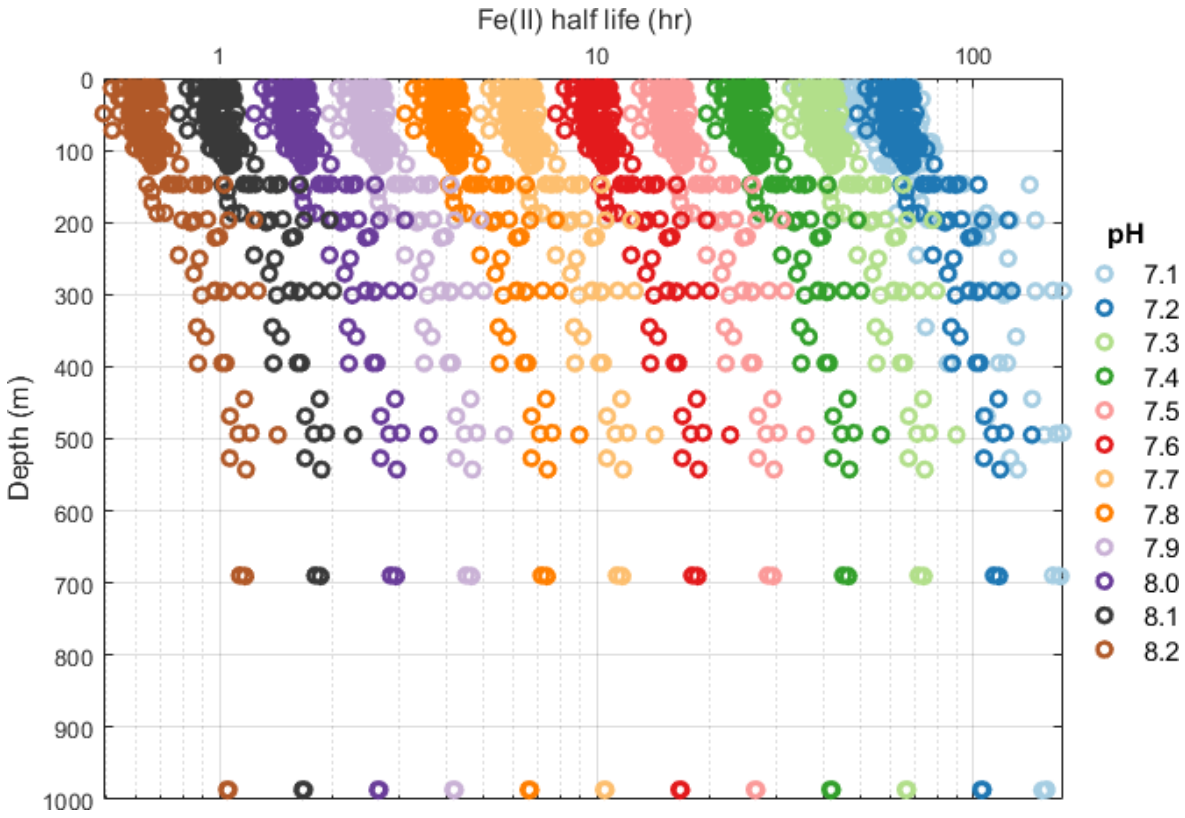

Figure 5. Scatter plot of all Fe(II) samples showing effect of pH on Fe(II) half-life, calculated from in-situ DFe(II), H_2O_2 and O_2 measurements. The pH range reflects upper and lower bounds of observations made during historical hydrographic voyages in the region, taken from the World Ocean Database (Tanhua et al., 2013).

4. Discussion

Dissolved Fe(II) concentrations as high as 0.57 nmol L^{-1} were measured in waters north of Heard Island and 1.01 nmol L^{-1} to the east of McDonald Islands. These concentrations are

higher than most existing DFe(II) measurements in open Southern Ocean surface waters, which are generally below 0.03 nmol L^{-1} (Bowie et al., 2002; Sarthou et al., 2011). Peroxide concentrations around HIMI (13.5 – 31.0 nmol L^{-1}) were low relative to concentrations found in lower latitude regions of the ocean (e.g. 300 nmol L^{-1}; Yuan and Shiller, 2001), but consistent with the closest Southern Ocean observations taken ~700 km west of the Kerguelen Plateau (4.9 – 20.2 nmol L^{-1}; Sarthou et al., 1997).

Sources of DFe(II) near HIMI may include benthic fluxes from anoxic and sub-oxic sediments (Lohan and Bruland, 2008), hydrothermal fluids (Holmes et al., 2017), glacial runoff (Raiswell et al., 2018) and atmospheric deposition of aerosols (Croot and Heller, 2012). Additional production mechanisms of DFe(II) in the surface ocean include photochemistry, through the breakdown and reduction of Fe(III)-ligand complexes (Rijkenberg et al., 2005) and biological production, through bioreduction of Fe(III)-ligand complexes, grazing or viral lysis of cells (Hansard et al., 2009). We now discuss each of these sources in relation to data collected during the HEOBI voyage in order to identify potential influences on the elevated Fe(II) concentrations observed in the region.

4.1. Glacial runoff

At Heard Island, glacial runoff appears to be the most important source of Fe(II), with evidence suggesting that the elevated DFe(II) signal at station 24 originates from Heard Island glacial meltwaters. Comparing DFe(II) concentrations with salinity at stations north of Heard Island suspected of being influenced by glacial processes (stations 24, 23 and 36 – 40) shows a significant inverse correlation ($R^2 = 0.57$, $P < 0.01$; Figure 6). Samples taken at the station in front of Downes and Ealey marine terminating glaciers (station 24) are distinct from the other Heard Island samples, higher DFe(II) concentrations (mean 0.53 nmol L^{-1}) compared to nearby stations (mean DFe(II) 0.18 nmol L^{-1} at stations 36 – 40).

316 The percentage of DFe(II) relative to DFe(total) can indicate the presence of a strong Fe(II)
317 source (e.g. Sedwick et al., 2015). Dissolved Fe(II) concentrations at the Heard Island station
318 closest to Downes and Ealey glaciers (station 24) were an order of magnitude higher than
319 those observed at the reference station (below detection – 0.05 nmol L^{-1} range in the upper
320 100 m), i.e. regional open ocean conditions (Figure 3). Mean DFe(II) percentage over the
321 water column at station 24 was also high at 25% (Figure 7). This enrichment in DFe(II)
322 suggests that there was a strong DFe(II) source adjacent to the glacial outflow, which
323 supported the elevated concentrations observed to the north of Heard Island in well
324 oxygenated waters (median 328 µmol L^{-1} O_2).

325 High DFe(II) (0.44 nmol L^{-1}) and DFe (1.88 nmol L^{-1}) concentrations were also observed in
326 the upper 30 m downstream to the east (7 km) of station 24 (station 23, Figure 3), where
327 targeted sampling was undertaken based on a large acoustic plume (Spain et al., 2019). This
328 area was later revisited and sampled in a crosshair pattern (stations 36 – 40) in an attempt to
329 delineate the signal source. However, these crosshair stations yielded lower DFe(II) and DFe
330 concentrations (mean 0.15 ± 0.1 and 1.53 ± 0.19 nmol L^{-1}, n = 21, respectively) compared to
331 the elevated samples observed previously (station 23) or further to the west, towards the
332 glacier terminus (station 24). The two samples in the upper 30 m of station 23 were also
333 associated with water that was lower in salinity and higher in DFe(II) than revisited crosshair
334 stations 36 – 40, but slightly lower in DFe(II) than station 24 samples. This is likely laterally
335 advected, glacially influenced surface water that has diluted with distance from the Heard
336 Island source. Indeed, particle laden waters advecting away from Heard Island are visible in
337 satellite imagery of the region (van der Merwe et al., 2019). Furthermore, previous studies
338 have shown that glacial erosion and melting results in runoff enriched with DFe (Raiswell et
339 al., 2018). 'Dissolved' iron may also include particles <0.4 µm, including Fe(II)-enriched
340 nanoparticles (Hawkings et al., 2018; Shoenfelt et al., 2017), from which DFe(II) may be

released and stabilised by ligands (Hawkings et al., 2018; Hopwood et al., 2014) or potentially consumed directly as particles (Shoenfelt et al., 2017).

Suspended particulate analysis from the HEOBI voyage provides additional evidence that waters to the north of Heard Island are influenced by glacial runoff (van der Merwe et al., 2019). Immediately adjacent to the large marine terminating glacier on the north of Heard Island, suspended particles were found to be highly labile, with higher proportions of Fe oxyhydroxide nanoparticles, in contrast to less-labile, lithogenic Fe bearing mineral particles observed at McDonald Islands (van der Merwe et al., 2019). Iron oxyhydroxide nanoparticles can be formed from DFe(II) and can produce DFe(II) through dissolution enhanced by photochemical reduction and grazing (Raiswell, 2011). This could be an important mechanism in maintaining the observed DFe(II) and DFe enrichment at Heard Island.

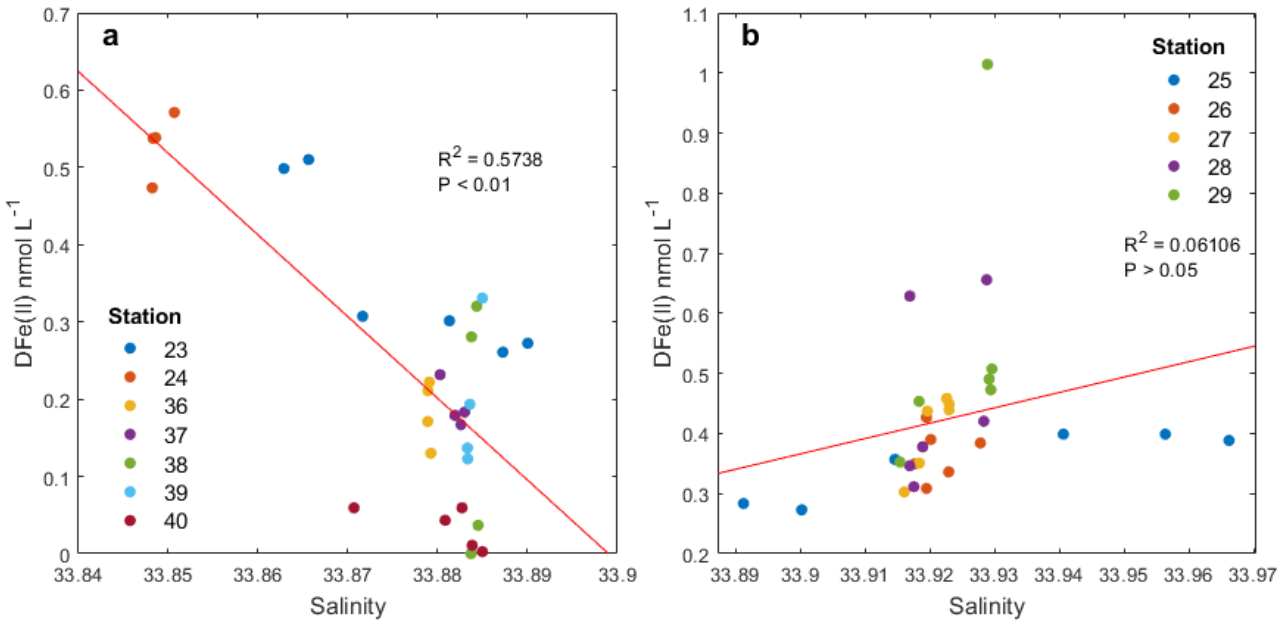

Figure 6. DFe(II) versus Salinity at **a.** Heard Island station 24 and crosshair stations 23, 36 – 40 and **b.** McDonald Islands crosshair stations 25 – 29. Station numbers are annotated.

4.2. Hydrothermal and sedimentary sources

At McDonald Islands, hydrothermal inputs appear to be the most important source of Fe(II), with evidence suggesting that the elevated DFe(II) signal at stations 28 and 29 originated

from diffuse hydrothermal sources. Numerous acoustic flare signals detected by ship-board echosounder and footage of bubbles emanating from the seafloor (Figure 8) at several locations around HIMI, were clues that hydrothermal vents were present in the region. The presence of localised DFe(II) maxima (Figure 3), elevated DFe(II) to DFe(total) ratios (Figure 7), sharp DFe(II) spikes in the water column (Figure 9), along with observations of excess ^{3}He with clear hydrothermal origins (Lupton et al., 2017), indicate that shallow water (<200 m) hydrothermalism was a likely source of DFe(II) at stations west of McDonald Islands.

The first clue that hydrothermalism may be a dominant source of DFe(II) at McDonald Islands is the presence of localised elevated DFe(II) maxima. Five stations (25 – 29) were sampled to the east of McDonald Islands in a 'crosshair' pattern (Figure 1). These sampling locations were selected in an attempt to further delineate elevated DFe concentrations detected at a previous station (station 12; Holmes et al., 2019) and where strong acoustic flare signals were observed (Spain et al., 2019). Mean DFe(II) concentrations at the McDonald crosshair stations were significantly higher (t-test, $P < 0.01$; Figure 9c) than the Heard crosshair stations, and exhibited pronounced spikes in DFe(II) at various depths at two of the stations.

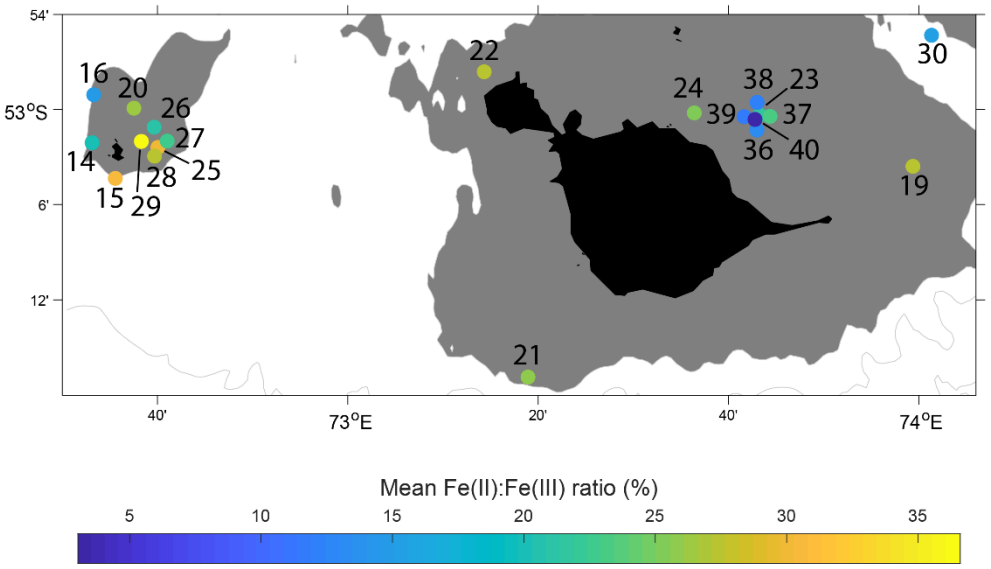

375

376 Figure 7. Mean Fe(II) to Fe(III) percentage over the water column for each station near Heard and McDonald Islands. Note
377 that station 20 is omitted as data are at detection limits, giving a falsely high ratio.

378 The station closest to McDonald Islands at the western side of the crosshair (station 29), had
379 the greatest DFe(II) concentration and DFe(II):DFe(total) percentage observed during
380 HEOBI (1.01 nmol L^{-1} and 37%, respectively; Figure 7). The next highest maximum DFe(II)
381 concentration (0.66 nmol L^{-1}) was observed at the southernmost crosshair station (station 28).
382 These stations were separated by a distance of 780 m and ~1.5 hours between sampling.
383 These spikes in maximum DFe(II) concentrations, located at varying depths, were unusual
384 compared to other stations around HIMI (Figure 3). The other three stations of the crosshair
385 (25, 26 and 27; 630 m east-southeast, 730 m northeast and 1040 m east from station 29,
386 respectively) had lower overall DFe(II) concentrations and were more homogeneous over the
387 water column (0.27 – 0.40, 0.31 – 0.43 and 0.30 – 0.46 nmol L^{-1}, respectively). The existence
388 of profiles with pronounced spikes in DFe(II) concentrations and profiles with homogenous
389 DFe(II) among the closely spaced crosshair stations may attest to the turbulent mixing and
390 rapidly oxidising conditions in the region and indicates that the DFe(II) originates from point
391 source(s) such as a vent or patch, rather than a larger area of the seafloor, such as might be
392 expected from benthic flux.

Figure 8. Bubbles rising from the seafloor at a site NE of Heard Island, captured using deep tow camera during the HEOBI voyage. Though plumes were detected using echosounder around both islands, no bubble plumes were captured on camera near McDonald Islands. Photo courtesy of the Marine National Facility, CSIRO.

The presence of DFe(II) peaks at various depths in the water column at the two stations (28, 29) with the most elevated DFe(II) could indicate that TMR casts intercepted point source plumes as the ship and/or rising plumes moved laterally with currents (e.g. Bennett et al., 2009). Due to the turbulent nature of waters surrounding HIMI, and the point source nature of the observed elevated DFe(II) concentrations at the McDonald Islands crosshair stations, it is unlikely that a TMR cast would stay within a plume for the duration of the cast (~1 hour). A DFe(II) point source would also make sampling directly above the source challenging without a remotely operated vehicle.

Sediments are another potential DFe(II) source in the HIMI region. Relatively high particle backscattering was observed around HIMI (Wojtasiewicz et al., 2019) and wind-driven mixing events often reached the seafloor around HIMI during the voyage resulting in a well-mixed water column homogeneous in properties such as temperature and salinity (R. Robertson, pers. comm.). This mixing could disturb upper oxidising sediment layers, resuspend sediments and potentially facilitate the escape of Fe(II) from underlying anoxic sediments (e.g. Elrod et al., 2004). However, with the exception of stations 15 and 21, no obvious maximum in DFe(II) was observed near the seafloor as would be expected if

sedimentary sources dominated (Figure 3). Sediments on continental shelves have been identified as strong DFe(II) sources, especially in the presence of hypoxic bottom waters (Lohan and Bruland, 2008). In the presence of oxygenated bottom waters, the upper layer of sediment tends to form an oxidising barrier, meaning relatively little DFe(II) can penetrate into the overlying water column (Homoky et al., 2016). However, an example of benthic flux of Fe(II) to oxygenated bottom waters has been observed in a region of hydrothermal activity in the Bransfield Straight, Southern Ocean (Aquilina et al., 2014). This flux was attributed to infaunal tubeworms, the remains of which provided conduits for subsurface fluid to bypass the upper sediment layer (Aquilina et al., 2014). Though there was no biologically focused sampling program during the HEOBI voyage, bioturbation of surface sediments is likely, due to the shallow bathymetry and biological productivity in the region – including a rich diversity of benthic species (Améziane et al., 2011). However, If the source of elevated DFe(II) at the McDonald crosshair stations was sedimentary in origin, we would expect to see an increase in concentrations towards the seafloor over a larger area (Lohan and Bruland, 2008), which was not observed during HEOBI.

Numerous observations via deep tow camera of bubbles emitted from seafloor vents scattered around the entire region during the HEOBI voyage (Figure 8) and recent δ^3He anomaly data (an unequivocal tracer of hydrothermalism; Lupton et al., 2017) add further evidence that diffuse hydrothermal venting is a likely source of DFe(II) at McDonald Islands. The greatest δ^3He enrichment (10.1%) in the region was observed in the vicinity of the crosshair station group near McDonald Islands,

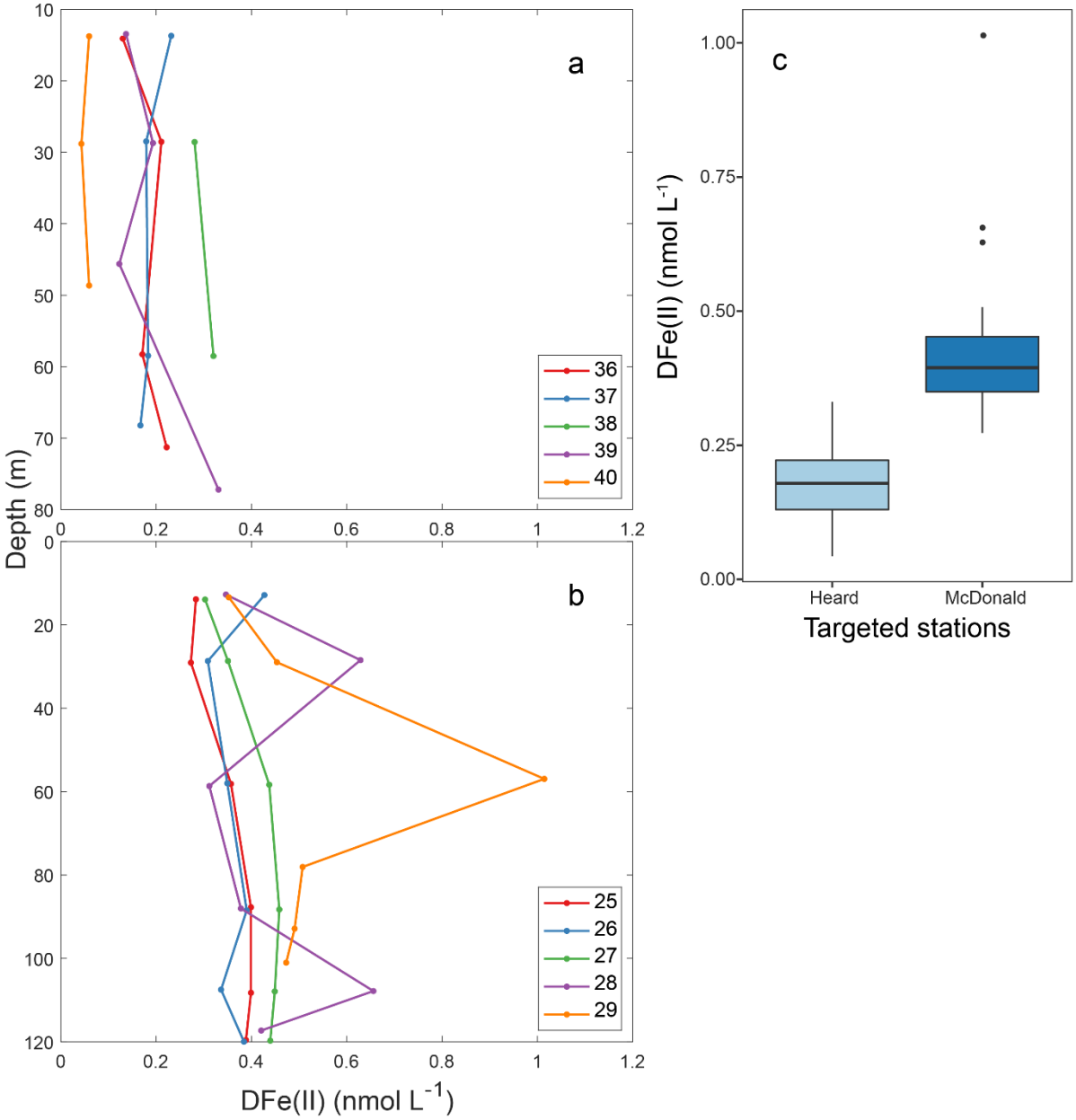

Figure 9. DFe(II) versus depth at **a.** Heard Island crosshair stations (36 – 40) and **b.** McDonald Islands crosshair stations 25 – 29. Station numbers are annotated. Note that due to analytical constraints, replicate measurements were unavailable for some samples. Therefore, given the well mixed nature of the water around both islands, data from each of the crosshair sites has been summarised in **c.** boxplots. The bottom and top limits of the boxes represent the 25th and 75th percentiles, respectively. The horizontal line within the box represents the median. The lower and upper whiskers extend from the 25th and 75th percentiles to the lowest and highest values within the interquartile range, respectively. Solid circles represent outlying values. Data lower than detection limits have been excluded.

compared to 1.7% close to station 37, near the northeast of Heard Island (Lupton et al., 2017). Acoustic flares, detected by the shipboard echosounder, were observed at both Heard and McDonald Islands (Spain et al., 2019). This may suggest that while there were stronger glacial sources of DFe(II) at Heard Island, hydrothermalism may have contributed to elevated

446 background concentrations observed around both islands, along with sedimentary and other
447 sources (discussed below).

448 ### 4.3. Other DFe(II) sources and sinks

449 Photochemical processes, H_2O_2 and O_2 concentrations, atmospheric deposition of wet and dry
450 aerosols, biological processes and changes in seawater pH all represented potential sources
451 and sinks in the HIMI region during HEOBI. Production of Fe(II) through photochemical
452 processes did not appear to be the strongest influence of DFe(II) concentrations around HIMI,
453 as comparison of shipboard surface photosynthetically active radiation (PAR) observations
454 with surface DFe(II) concentrations showed no correlation (Figure S1). Surface H_2O_2
455 concentrations also showed no correlation with PAR (Figure S1); however, concentrations in
456 surface waters were correlated with distance from land ($R^2 = 0.70$, $P < 0.01$), with greatest
457 surface H_2O_2 observed at stations furthest from HIMI (i.e. stations 9 and 10 on the central
458 northern plateau and 30 – 35 on transect C; Figure 3, 4). These stations were deeper and
459 could thus form a stratified surface mixed layer, allowing H_2O_2 to accumulate above the
460 pycnocline. Surface H_2O_2 showed a weak relationship ($R^2 = 0.18$, $n = 26$) with surface DFe(II)
461 concentrations (Figure S2). The low H_2O_2 concentrations and lack of correlation between
462 DFe(II) and either H_2O_2, O_2, or PAR around HIMI suggests that on-plateau DFe(II)
463 distributions are predominantly governed by strong local DFe(II) sources.

464 Atmospheric deposition did not appear to be a major source of dissolved or particulate Fe
465 during HEOBI, and therefore not a major source of DFe(II), as DFe(II) represents a fraction
466 of total Fe. Wet deposition of DFe(II) and H_2O_2 was not apparent (Figure S1), possibly
467 because of the minimal precipitation during HEOBI. The mean aerosol soluble Fe observed
468 during HEOBI (0.30 ± 0.12 ng m^{-3}; $n = 13$, M. M. G. Perron, pers. comm.) was on the same
469 order as values found near Kerguelen Island to the north (0.29 ± 0.14 ng m^{-3}; Blain et al.,
470 2008), which were not deemed to be a significant source of DFe to that region (Blain et al.,

2008). These values also fall in the range of baseline Southern Ocean aerosol soluble Fe (0.01 – 0.3 ng m^{-3}; Winton et al., 2015), where surface concentrations of DFe(II) are reported to range from below detection to 30 pmol L^{-1}. Thus, we can assume that the contribution of dry deposition aerosols to DFe(II) observations in the water column is probably minor.

Biological production by processes such as viral lysis of cells and grazing (Hansard et al., 2009 and references therein) likely contributed to background DFe(II) concentrations in waters around HIMI. While no direct observations were taken to enable an estimate of the biological production of DFe(II) during HEOBI, it can be inferred from our observations that biological production was not the greatest source of elevated DFe(II) observed near Heard or McDonald Islands. Indeed, Wojtasiewicz et al. (2019) showed that during HEOBI phytoplankton communities around HIMI were limited by low light availability due to deep mixing and shading by re-suspended sediment particles and augmented by dilution with surrounding low chlorophyll waters of the Antarctic Circumpolar Current.

In addition, pH and temperature conditions should be considered in relation to Fe(II) half-life in the HIMI region. Low temperatures, such as those found in waters around HIMI, extend Fe(II) half-life in high-latitude waters by slowing oxidation reactions (Croot et al., 2001). Our modelling results show that pH has a significant impact on Fe(II) half-life (Figure 5). Using in-situ observations of variables required in the equations and changing pH in steps of 0.1 units shows the strong dependence of Fe(II) half-life on pH (Figure 5). These results indicate that input of low pH fluids from diffuse hydrothermal sources could dramatically impact Fe(II) speciation and half-life close to vent sources.

Aerosol deposition, biological production and photochemical processes were not the strongest sources of DFe(II) in the HIMI region. However, it is likely that these sources, coupled with low water temperature and possibly localised lower pH in areas of the region,

contributed to the overall elevated DFe(II) concentrations observed at stations in the HIMI region.

4.4. Fe(II) transport

Using current velocities observed during HEOBI (R. Robertson, pers. comm.) and previous voyages (Park et al., 2008), and our modelled Fe(II) half-lives, a rough estimate of the distance Fe(II) might travel from HIMI can be calculated. Modelled half-lives ranged from 30 minutes to 172 hours. Current velocities over the plateau were slow (~6 cm s^{-1}), while currents to the east of Heard Island were stronger (~40 cm s^{-1}), in agreement with previous observations (Park et al., 2008). Both currents over the plateau and to the east of Heard Island flowed in a northerly direction. Using these figures, the distance Fe(II) could theoretically travel in one half-life over the plateau ranged from ~100 m to ~37 km. If Fe(II) reached the stronger currents to the east of Heard Island, in one half-life Fe(II) could theoretically travel between ~700 m and ~250 km. Considering that the greatest Fe(II) concentration observed at HIMI (~1 nmol L^{-1}) will take approximately 5 half-lives to reach surface Southern Ocean background concentrations (~0.03 nmol L^{-1}; Sarthou et al., 2011), it is plausible that Fe(II) from hydrothermal and glacial sources at HIMI could travel the distances required to fertilise the phytoplankton plume that forms over the plateau annually. This may have implications for future Fe supply to the northern plateau, since under warming climate conditions, melting glacial waters may increase, potentially increasing the supply of DFe(II), and could then rapidly decrease once glaciers have melted.

5. Conclusion

We show that the strongest sources of DFe(II) differ between adjacent, volcanically active Heard and McDonald Islands. Maximum DFe(II) concentrations and varying mid-depth maxima in the water column at adjacent, targeted stations at McDonald Islands suggest that

519 hydrothermalism is the strongest DFe(II) source. At Heard Island, the strongest DFe(II)
520 source correlates with low salinity waters and is near a marine-terminating glacier, suggesting
521 that glacial meltwater (and possibly associated glacial flour) is the major source of DFe(II).
522 Revisited stations to the east of the strongest signal showed a temporary freshwater and
523 elevated DFe(II) signal, which suggests that glacially fertilised waters may be transported
524 offshore from Heard Island. These results are in agreement with preliminary δ^3He (Lupton et
525 al., 2017) and particulate Fe data (van der Merwe et al., 2019) also collected during the
526 HEOBI voyage.

527 Peroxide and PAR data shows that neither H_2O_2 or PAR correlate with DFe(II)
528 concentrations around HIMI, suggesting that on-plateau DFe(II) concentrations are
529 predominantly governed by strong local DFe(II) sources. Preliminary aerosol data collected
530 during the HEOBI voyage confirms that soluble aerosol concentrations were low. The
531 homogenous nature of most DFe(II) and H_2O_2 profiles around HIMI highlights the strong
532 mixing regime in the region but obscures some features that would allow direct attribution to
533 a source. Further research is necessary to determine exact mechanisms of decay and/or
534 consumption of DFe(II) in the water column. In addition to the strong sources from
535 hydrothermal and glacial inputs identified in this study, the overall elevated concentrations of
536 DFe(II) around HIMI are likely to be an accumulation of multiple sources (sedimentary
537 resuspension, surface irradiance, biological production and atmospheric deposition), in
538 addition to opposing controls on DFe(II) half-life from low temperature, highly oxygenated
539 waters and potentially lower pH, which have all been homogenised in the well mixed water
540 column. The elevated concentrations of DFe(II) around HIMI, a highly labile and
541 bioavailable form of Fe, may increase Fe availability for biota in the region. High DFe(II)
542 concentrations may also indicate slower oxidation kinetics in the region, which has

implications for transport of Fe away from the islands to the broader northern Kerguelen Plateau where the annual plankton bloom is strongest.

6. Acknowledgements

The authors would like to thank Rob Middag (University of Otago, New Zealand) for supplying the FIA-CL instrument that was used to analyse H_2O_2 samples during the voyage, Manon Tonnard (Laboratoire des sciences de l'Environnement MARin: LEMAR) and Lavenia Ratnarajah (Antarctic Climate and Ecosystems Cooperative Research Centre and Institute for Marine and Antarctic Studies: ACECRC, IMAS) for their assistance in collecting and filtering samples on the HEOBI voyage. We would like to thank Mark Rayner and Kendall Sherrin for their excellent oxygen analyses. We also thank the captain, officers and crew of the RV Investigator (HEOBI voyage) and Chief Scientist Mike Coffin for their support during the 53-day expedition. We wish to acknowledge the Australian Research Council (DP150100345 and LE0989539), the Australian Antarctic Science Program (AAS4338) and the Australian Government Cooperative Research Centres Program through the Antarctic Climate and Ecosystems CRC, who provided project funding and PhD scholarship support. Dissolved Fe(II) and H_2O_2 data are publicly available online in the CSIRO data repository (https://doi.org/COMINGSOON) and will also be available in the GEOTRACES 2021 Intermediate Data Product.

7. References

Améziane, N., Eléaume, M., Hemery, L.G., Monniot, F., Hemery, A., Hautecoeur, M., Dettaï, A., 2011. Biodiversity of the benthos off Kerguelen Islands : overview and perspectives. Kerguelen Plateau Mar. Ecosyst. Fish. 157–167.

Aquilina, A., Homoky, W.B., Hawkes, J.A., Lyons, T.W., Mills, R.A., 2014. Hydrothermal sediments are a source of water column Fe and Mn in the Bransfield Strait, Antarctica.

567 Geochim. Cosmochim. Acta 137, 64–80. doi:10.1016/j.gca.2014.04.003

568 Bennett, S.A., Rouxel, O., Schmidt, K., Garbe-Schönberg, D., Statham, P.J., German, C.R.,
569 2009. Iron isotope fractionation in a buoyant hydrothermal plume, 5°S Mid-Atlantic
570 Ridge. Geochim. Cosmochim. Acta 73, 5619–5634. doi:10.1016/j.gca.2009.06.027

571 Blain, S., Quéguiner, B., Armand, L., Belviso, S., Bombled, B., Bopp, L., Bowie, A., Brunet,
572 C., Brussaard, C., Carlotti, F., Christaki, U., Corbière, A., Durand, I., Ebersbach, F.,
573 Fuda, J.-L., Garcia, N., Gerringa, L., Griffiths, B., Guigue, C., Guillerm, C., Jacquet, S.,
574 Jeandel, C., Laan, P., Lefèvre, D., Lo Monaco, C., Malits, A., Mosseri, J., Obernosterer,
575 I., Park, Y.-H., Picheral, M., Pondaven, P., Remenyi, T., Sandroni, V., Sarthou, G.,
576 Savoye, N., Scouarnec, L., Souhaut, M., Thuiller, D., Timmermans, K., Trull, T., Uitz, J.,
577 van Beek, P., Veldhuis, M., Vincent, D., Viollier, E., Vong, L., Wagener, T., 2007.
578 Effect of natural iron fertilization on carbon sequestration in the Southern Ocean. Nature
579 446, 1070–4. doi:10.1038/nature05700

580 Blain, S., Sarthou, G., Laan, P., 2008. Distribution of dissolved iron during the natural iron-
581 fertilization experiment KEOPS (Kerguelen Plateau, Southern Ocean). Deep Sea Res.
582 Part II Top. Stud. Oceanogr. 55, 594–605. doi:10.1016/j.dsr2.2007.12.028

583 Bowie, A.R., Achterberg, E.P., Sedwick, P.N., Ussher, S., Worsfold, P.J., 2002. Real-Time
584 Monitoring of Picomolar Concentrations of Iron (II) in Marine Waters Using Automated
585 Flow Instrumentation. Environ. Sci. Technol. 36, 4600–4607. doi:10.1021/es020045v

586 Bowie, A.R., Achterberg, E.P., Ussher, S., Worsfold, P.J., 2005. Design of an automated flow
587 injection-chemiluminescence instrument incorporating a miniature photomultiplier tube
588 for monitoring picomolar concentrations of iron in seawater. J. Autom. Methods Manag.
589 Chem. 2005, 37–43. doi:10.1155/JAMMC.2005.37

590 Bowie, A.R., Sedwick, P.N., Worsfold, P.J., 2004. Analytical intercomparison between flow

injection-chemiluminescence and flow injection-spectrophotometry for the determination of picomolar concentrations of iron in seawater. Limnol. Oceanogr. Methods 2, 42–54. doi:10.4319/lom.2004.2.42

Boyd, P.W., Ellwood, M.J., 2010. The biogeochemical cycle of iron in the ocean. Nat. Geosci. doi:10.1038/ngeo964

Boyd, P.W., Jickells, T., Law, C.S., Blain, S., Boyle, E. a, Buesseler, K.O., Coale, K.H., Cullen, J.J., de Baar, H.J.W., Follows, M., Harvey, M., Lancelot, C., Levasseur, M., Owens, N.P.J., Pollard, R., Rivkin, R.B., Sarmiento, J., Schoemann, V., Smetacek, V., Takeda, S., Tsuda, a, Turner, S., Watson, a J., 2007. Mesoscale iron enrichment experiments 1993-2005: synthesis and future directions. Science 315, 612–7. doi:10.1126/science.1131669

Cohan, D.S., Schultz, M.G., Jacob, D.J., Heikes, B.G., Blake, D.R., 1999. Convective injection and photochemical decay of peroxides in the tropical upper troposphere: Methyl iodide as a tracer of marine convection. J. Geophys. Res. Atmos. 104, 5717–5724. doi:10.1029/98JD01963

Croot, P.L., Bowie, A.R., Frew, R.D., Maldonado, M.T., Hall, J.A., Safi, K.A., La Roche, J., Boyd, P.W., Law, C.S., 2001. Retention of dissolved iron and Fe II in an iron induced Southern Ocean phytoplankton bloom. Geophys. Res. Lett. 28, 3425–3428. doi:10.1029/2001GL013023

Croot, P.L., Heller, M.I., 2012. The importance of kinetics and redox in the biogeochemical cycling of iron in the surface ocean. Front. Microbiol. 3, 219. doi:10.3389/fmicb.2012.00219

Croot, P.L., Streu, P., Peeken, I., Lochte, K., Baker, A.R., 2004. Influence of the ITCZ on H2O2 in near surface waters in the equatorial Atlantic Ocean. Geophys. Res. Lett. 31,

615 1–4. doi:10.1029/2004GL020154

616 Cutter, G., Andersson, P., Codispoti, L., Croot, P., Francois, R., Lohan, M., Obata, H.,
617 Rutgers, M., 2014. Sampling and Sample-handling Protocols for GEOTRACES Cruises.

618 Elrod, V. a., Berelson, W.M., Coale, K.H., Johnson, K.S., 2004. The flux of iron from
619 continental shelf sediments: A missing source for global budgets. Geophys. Res. Lett. 31,
620 n/a-n/a. doi:10.1029/2004GL020216

621 Hansard, S.P., Landing, W.M., Measures, C.I., Voelker, B.M., 2009. Dissolved iron(II) in the
622 Pacific Ocean: Measurements from the PO2 and P16N CLIVAR/CO_2 repeat
623 hydrography expeditions. Deep. Res. Part I Oceanogr. Res. Pap. 56, 1117–1129.
624 doi:10.1016/j.dsr.2009.03.006

625 Hawkes, J.J.A., Connelly, D.P., Rijkenberg, M.J.A., Achterberg, E.P., 2014. The importance
626 of shallow hydrothermal island arc systems in ocean biogeochemistry. Geophys. Res.
627 Lett. 41, 942–947. doi:10.1002/2013GL058817

628 Hawkings, J.R., Benning, L.G., Raiswell, R., Kaulich, B., Araki, T., Abyaneh, M., Stockdale,
629 A., Koch-müller, M., Wadham, J.L., Tranter, M., 2018. Biolabile ferrous iron bearing
630 nanoparticles in glacial sediments. Earth Planet. Sci. Lett. 493, 92–101.
631 doi:10.1016/j.epsl.2018.04.022

632 Holmes, T.M., Chase, Z., Van Der Merwe, P., Townsend, A.T., Bowie, A.R., 2017. Detection,
633 dispersal and biogeochemical contribution of hydrothermal iron in the ocean. Mar.
634 Freshw. Res. 68, 2184–2204. doi:10.1071/MF16335

635 Holmes, T.M., Wuttig, K., Chase, Z., van der Merwe, P., Townsend, A.T., Schallenberg, C.,
636 Tonnard, M., Bowie, A.R., 2019. Iron availability influences nutrient drawdown in the
637 Heard and McDonald Islands region, Southern Ocean. Mar. Chem. 211, 1–14.

638 doi:10.1016/j.marchem.2019.03.002

639 Homoky, W.B., Weber, T., Berelson, W.M., Conway, T.M., Henderson, G.M., van Hulten,
640 M., Jeandel, C., Severmann, S., Tagliabue, A., 2016. Quantifying trace element and
641 isotope fluxes at the ocean–sediment boundary: a review, Philosophical Transactions of
642 the Royal Society A: Mathematical, Physical and Engineering Sciences.
643 doi:10.1098/rsta.2016.0246

644 Hopwood, M.J., Statham, P.J., Tranter, M., Wadham, J.L., 2014. Glacial flours as a potential
645 source of Fe(II) and Fe(III) to polar waters. Biogeochemistry 118, 443–452.
646 doi:10.1007/s10533-013-9945-y

647 Hwang, H., Dasgupta, P.K., 1985. Thermodynamics of the hydrogen peroxide-water system.
648 Environ. Sci. Technol. 19, 255–258. doi:10.1021/es00133a006

649 Lohan, M.C., Bruland, K.W., 2008. Elevated Fe(II) and dissolved Fe in hypoxic shelf waters
650 off Oregon and Washington: An enhanced source of iron to coastal upwelling regimes.
651 Environ. Sci. Technol. 42, 6462–6468. doi:10.1021/es800144j

652 Lupton, J.E., Arculus, R.J., Coffin, M., Bradney, A., Baumberger, T., Wilkinson, C., 2017.
653 Hydrothermal venting on the flanks of Heard and McDonald islands, southern Indian
654 Ocean, in: AGU Fall Meeting Abstracts. p. V51F–0435.

655 Martin, J.H., Gordon, R.M., Fitzwater, S.E., 1990. Iron in Antarctic waters. Nature 345, 156–
656 158. doi:10.1038/345156a0

657 Millero, F.J., Sotolongo, S., 1989. The oxidation of Fe(II) with H2O2 in seawater. Geochim.
658 Cosmochim. Acta 53, 1867–1873. doi:10.1016/0016-7037(89)90307-4

659 Millero, F.J., Sotolongo, S., Izaguirre, M., 1987. The oxidation kinetics of Fe(II) in seawater.
660 Geochim. Cosmochim. Acta 51, 793–801. doi:10.1016/0016-7037(87)90093-7

661 Moore, C.M., Mills, M.M., Achterberg, E.P., Geider, R.J., LaRoche, J., Lucas, M.I.,
662 McDonagh, E.L., Pan, X., Poulton, A.J., Rijkenberg, M.J. a., Suggett, D.J., Ussher, S.J.,
663 Woodward, E.M.S., 2009. Large-scale distribution of Atlantic nitrogen fixation
664 controlled by iron availability. Nat. Geosci. 2, 867–871. doi:10.1038/ngeo667

665 Palenik, B., Morel, F.M.M., 1988. Dark production of H2O2 in the Sargasso Sea. Limnol.
666 Oceanogr. 33, 1606–1611. doi:10.4319/lo.1988.33.6part2.1606

667 Park, Y.Y.-H., Durand, I., Kestenare, E., Rougier, G., Zhou, M., d'Ovidio, F., Cotté, C., Lee,
668 J.-H., 2014. Polar Front around the Kerguelen Islands: An up-to-date determination and
669 associated circulation of surface/subsurface waters. J. Geophys. Res. Ocean. 1–18.
670 doi:10.1002/2014JC010061.Received

671 Park, Y.-H., Roquet, F., Durand, I., Fuda, J.-L., 2008. Large-scale circulation over and around the
672 Northern Kerguelen Plateau. Deep Sea Res. Part II Top. Stud. Oceanogr. 55, 566–581.
673 doi:10.1016/j.dsr2.2007.12.030

674 Raiswell, R., 2011. Iceberg-hosted nanoparticulate Fe in the Southern Ocean: Mineralogy,
675 origin, dissolution kinetics and source of bioavailable Fe. Deep. Res. Part II Top. Stud.
676 Oceanogr. 58, 1364–1375. doi:10.1016/j.dsr2.2010.11.011

677 Rijkenberg, M.J.A., Fischer, A.C., Kroon, J.J., Gerringa, L.J.A., Timmermans, K.R.,
678 Wolterbeek, H.T., De Baar, H.J.W., 2005. The influence of UV irradiation on the
679 photoreduction of iron in the Southern Ocean. Mar. Chem. 93, 119–129.
680 doi:10.1016/j.marchem.2004.03.021

681 Santana-Casiano, J.M., González-Dávila, M., Millero, F.J., 2006. The role of Fe(II) species
682 on the oxidation of Fe(II) in natural waters in the presence of O_2 and H_2O_2. Mar. Chem.
683 99, 70–82. doi:10.1016/j.marchem.2005.03.010

Sarthou, G., Bucciarelli, E., Chever, F., Hansard, S.P., González-Dávila, M., Santana-Casiano, J.M., Planchon, F., Speich, S., 2011. Labile Fe(II) concentrations in the Atlantic sector of the Southern Ocean along a transect from the subtropical domain to the Weddell Sea Gyre. Biogeosciences 8, 2461–2479. doi:10.5194/bg-8-2461-2011

Sarthou, G., Jeandel, C., Brisset, L., Amouroux, D., Besson, T., Donard, O.F.X., 1997. Fe and H2O2 distributions in the upper water column in the Indian sector of the Southern Ocean. Earth Planet. Sci. Lett. 147, 83–92. doi:10.1016/S0012-821X(97)00004-6

Sedwick, P.., Sohst, B.M., Ussher, S.J., Bowie, A.R., 2015. A zonal picture of the water column distribution of dissolved iron(II) during the U.S. GEOTRACES North Atlantic transect cruise (GEOTRACES GA03). Deep Sea Res. Part II Top. Stud. Oceanogr. 116, 166–175. doi:10.1016/j.dsr2.2014.11.004

Shaked, Y., Kustka, A.B., Morel, M.M., 2005. A general kinetic model for iron acquisition by eukaryotic phytoplankton. Limnol. Oceanogr. 50, 872–882.

Shoenfelt, E.M., Sun, J., Winckler, G., Kaplan, M.R., Borunda, A.L., Farrell, K.R., Moreno, P.I., Gaiero, D.M., Recasens, C., Sambrotto, R.N., Bostick, B.C., 2017. High particulate iron(II) content in glacially sourced dusts enhances productivity of a model diatom. Sci. Adv. 3. doi:10.1126/sciadv.1700314

Spain, E.A., Johnson, S.C., Hutton, B., Whittaker, J.M., Lucieer, V., Watson, S.J., Fox, J.M., Lupton, J., Arculus, R., Bradney, A., Coffin, M.F., 2019. Shallow seafloor gas emissions near Heard and McDonald Islands on the Kerguelen Plateau, southern Indian Ocean. Earth Sp. Sci. 1–19. doi:10.1029/2019ea000695

Tanhua, T., Olsen, A., Hoppema, M., Jutterström, S., Schirnick, C., van Heuven, S.M.A.C., Velo, A., Lin, X., Kozyr, A., Álvarez, M., Bakker, D.C.E., Brown, P.J., Falck, E., Jeansson, E., Lo Monaco, C., Ólafsson, J., Pérez, F.F., Pierrot, D., Ríos, A.F., Sabine,

C.L., Schuster, U., Steinfeldt, R., Stendardo, I., Anderson, L.G., Bates, N., Bellerby, R.G.J., Blindheim, J., Bullister, J.L., Gruber, N., Ishii, M., Johannessen, T., Jones, E.P., Köhler, J., Körtzinger, A., Metzl, N., Murata, A., Musielewicz, S., Omar, A.M., Olsson, K.A., de la Paz, M., Pfeil, B., Rey, F., Rhein, M., Skjelvan, I., Tilbrook, B., Wanninkhof, R., Mintrop, L., Wallace, D.W.R., Key, R.M., 2013. Dissolved inorganic carbon, alkalinity, pH, temperature, salinity, and other variables collected from profile observations using CTD, discrete bottles, and other instruments from October 7, 1977 to March 11, 2006 [WWW Document]. URL https://www.nodc.noaa.gov/OC5/SELECT/dbsearch/dbsearch.html (accessed 7.18.18).

van der Merwe, P., Wuttig, K., Holmes, T., Trull, T.W., Chase, Z., Townsend, A.T., Goemann, K., Bowie, A.R., 2019. High Lability Fe Particles Sourced From Glacial Erosion Can Meet Previously Unaccounted Biological Demand: Heard Island, Southern Ocean. Front. Mar. Sci. 6, 1–20. doi:10.3389/fmars.2019.00332

Watson, S.J., Coffin, M.F., Whittaker, J.M., Lucieer, V., Fox, J.M., Carey, R., Arculus, R.J., Bowie, A.R., Chase, Z., Robertson, R., Martin, T., Cooke, F., 2016. Submarine geology and geomorphology of active Sub-Antarctic volcanoes: Heard and McDonald Islands, in: AGU Fall Meeting Abstracts.

Weller, R., Schrems, O., 1993. H2O2 in the marine troposphere and seawater of the Atlantic Ocean (48°N - 63°S). Geophys. Res. Lett. 20, 125–128. doi:10.1029/93GL00065

Winton, V.H.L., Bowie, A.R., Edwards, R., Keywood, M., Townsend, A.T., van der Merwe, P., Bollhöfer, A., 2015. Fractional iron solubility of atmospheric iron inputs to the Southern Ocean. Mar. Chem. 177, 20–32. doi:10.1016/j.marchem.2015.06.006

Wojtasiewicz, B., Trull, T.W., Clementson, L., Davies, D.M., Patten, N.L., Schallenberg, C., Hardman-Mountford, N.J., 2019. Factors Controlling the Lack of Phytoplankton

Biomass in Naturally Iron Fertilized Waters Near Heard and McDonald Islands in the Southern Ocean. Front. Mar. Sci. 6. doi:10.3389/fmars.2019.00531

Yuan, J., Shiller, A.M., 2001. The distribution of hydrogen peroxide in the southern and central Atlantic ocean 48, 2947–2970.

Yuan, J., Shiller, A.M., 1999. Determination of subnanomolar levels of hydrogen peroxide in seawater by reagent-injection chemiluminescence detection. Anal. Chem. 71, 1975–1980. doi:10.1021/ac981357c

8. List of Figures

Figure 5. Scatter plot of all Fe(II) samples showing effect of pH on Fe(II) half-life, calculated from in-situ DFe(II), H_2O_2 and O_2 measurements. The pH range reflects upper and lower bounds of observations made during historical hydrographic voyages in the region, taken from the World Ocean Database *(Tanhua et al., 2013)*.

Figure 6. DFe(II) versus Salinity at **a.** Heard Island station 24 and crosshair stations 23, 36 – 40 and **b.** McDonald Islands crosshair stations 25 – 29. Station numbers are annotated.

Figure 7. Mean Fe(II) to Fe(III) percentage over the water column for each station near Heard and McDonald Islands. Note that station 20 is omitted as data are at detection limits, giving a falsely high ratio.

Figure 8. Bubbles rising from the seafloor at a site NE of Heard Island, captured using deep tow camera during the HEOBI voyage. Though plumes were detected using echosounder around both islands, no bubble plumes were captured on camera near McDonald Islands. Photo courtesy of the Marine National Facility, CSIRO.

Figure 9. DFe(II) versus depth at **a.** Heard Island crosshair stations (36 – 40) and **b.** McDonald Islands crosshair stations 25 – 29. Station numbers are annotated. Note that due to analytical constraints, replicate measurements were unavailable for some samples. Therefore, given the well mixed nature of the water around both islands, data from each of the crosshair sites has been summarised in **c.** boxplots. The bottom and top limits of the boxes represent the 25^{th} and 75^{th} percentiles, respectively. The horizontal line within the box represents the median. The lower and upper whiskers extend from the 25^{th} and 75^{th} percentiles to the lowest and highest values within the interquartile range, respectively. Solid circles represent outlying values. Data lower than detection limits have been excluded.

9. Supporting information

9.1. Figures

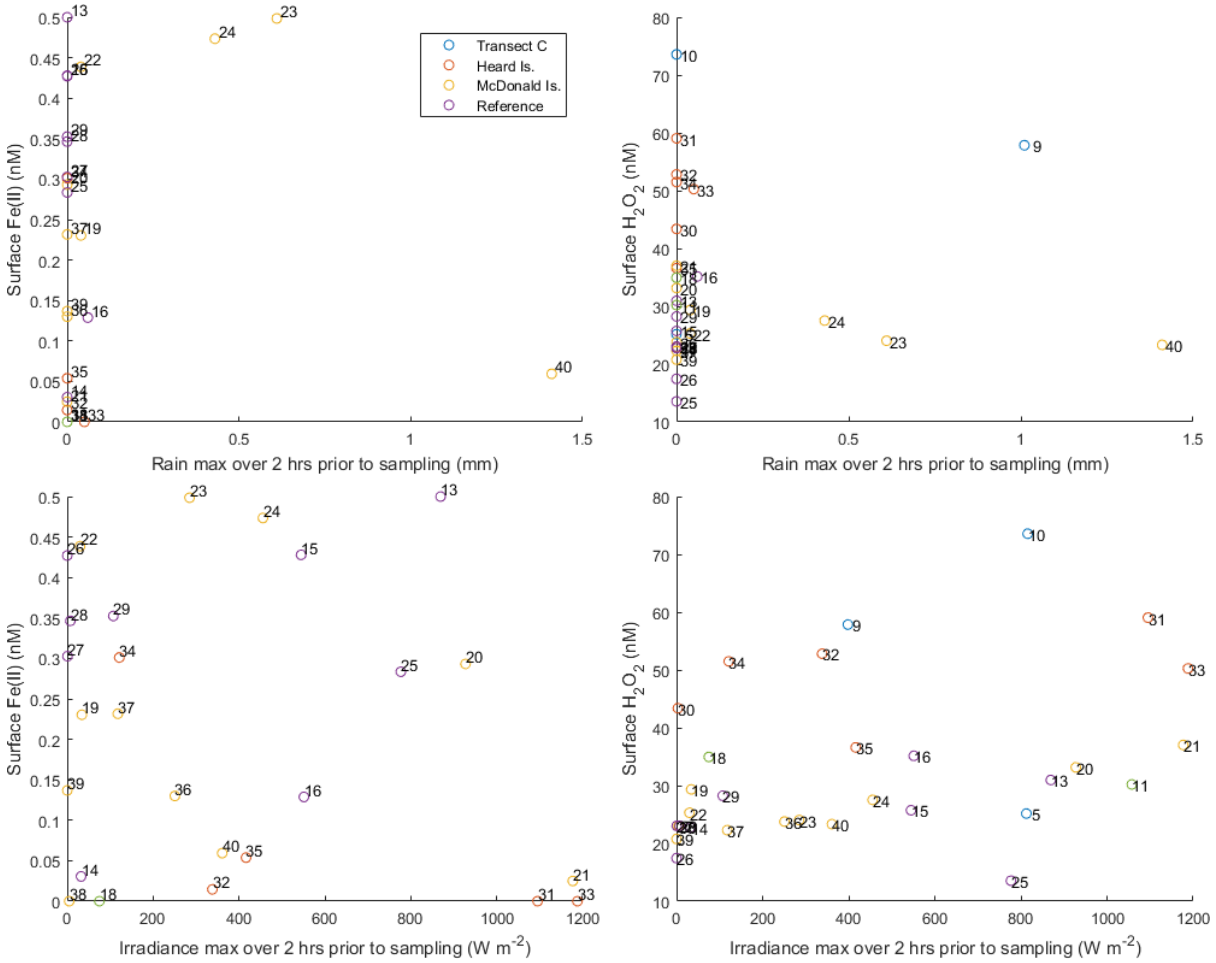

Figure S1. Surface DFe(II) and H_2O_2 vs maximum rainfall and maximum irradiance (PAR) over the 2 hours prior to sampling. Stations are annotated and colour coded by region.

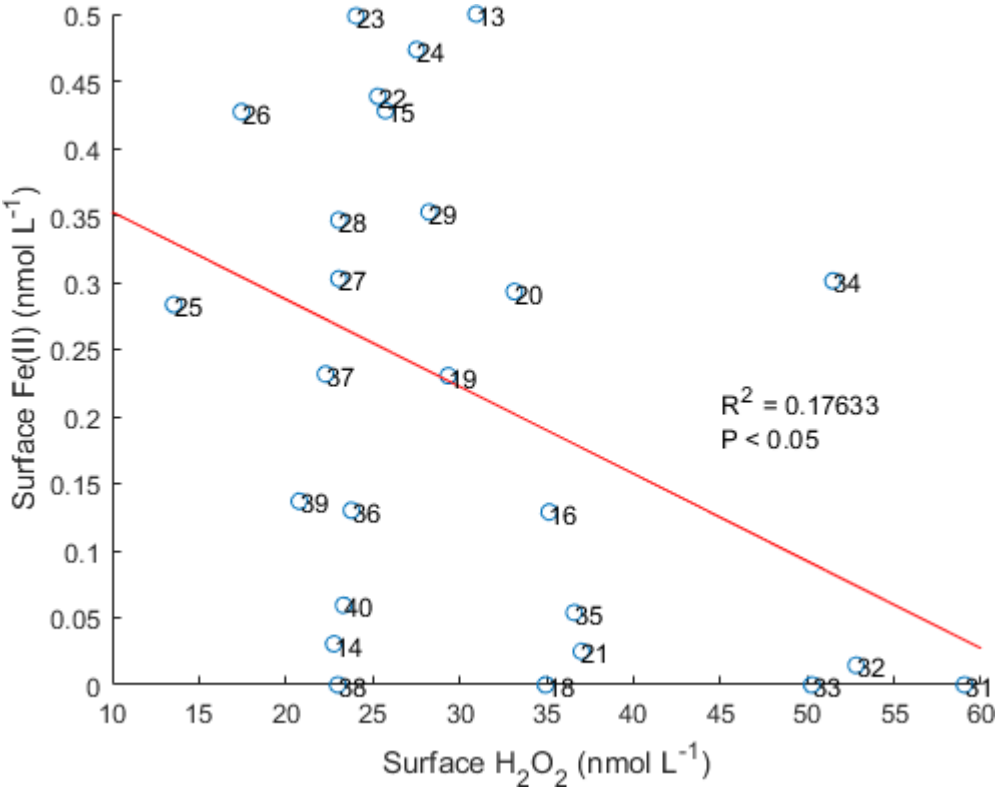

785

786 Figure S2. Surface DFe(II) vs surface H_2O_2 at all stations. Station numbers annotated.

GEOTRACE	Project	DATE_TIMI	TMR	BOTTLE_NI	LAT	LON	PRESSURE	Fe_II_D_CC	H2O2_D_C
GIpr05	HEOBI	########	2	12	-48.2798	79.36634	13.883	NaN	NaN
GIpr05	HEOBI	########	2	11	-48.2798	79.36634	28.616	NaN	NaN
GIpr05	HEOBI	########	2	10	-48.2798	79.36634	48.989	NaN	NaN
GIpr05	HEOBI	########	2	9	-48.2798	79.36634	68.699	NaN	NaN
GIpr05	HEOBI	########	2	8	-48.2798	79.36634	98.519	NaN	NaN
GIpr05	HEOBI	########	2	7	-48.2798	79.36634	148.284	NaN	NaN
GIpr05	HEOBI	########	2	6	-48.2798	79.36634	198.38	NaN	NaN
GIpr05	HEOBI	########	2	5	-48.2798	79.36634	298.326	NaN	NaN
GIpr05	HEOBI	########	2	4	-48.2798	79.36634	498.029	NaN	NaN
GIpr05	HEOBI	########	2	3	-48.2798	79.36634	697.813	NaN	NaN
GIpr05	HEOBI	########	2	2	-48.2798	79.36634	998.671	NaN	NaN
GIpr05	HEOBI	########	2	1	-48.2798	79.36634	1598.464	NaN	NaN
GIpr05	HEOBI	########	4	12	-50.24	77.72869	13.75	NaN	NaN
GIpr05	HEOBI	########	4	11	-50.24	77.72869	28.632	NaN	NaN
GIpr05	HEOBI	########	4	10	-50.24	77.72869	68.256	NaN	NaN
GIpr05	HEOBI	########	4	9	-50.24	77.72869	97.122	NaN	NaN
GIpr05	HEOBI	########	4	8	-50.24	77.72869	196.741	NaN	NaN
GIpr05	HEOBI	########	4	7	-50.24	77.72869	295.724	NaN	NaN
GIpr05	HEOBI	########	4	6	-50.24	77.72869	492.59	NaN	NaN
GIpr05	HEOBI	########	4	5	-50.24	77.72869	590.592	NaN	NaN
GIpr05	HEOBI	########	4	4	-50.24	77.72869	987.013	NaN	NaN
GIpr05	HEOBI	########	4	3	-50.24	77.72869	1971.293	NaN	NaN
GIpr05	HEOBI	########	4	2	-50.24	77.72869	2950.791	NaN	NaN
GIpr05	HEOBI	########	4	1	-50.24	77.72869	3317.002	NaN	NaN
GIpr05	HEOBI	########	5	12	-50.691	76.18671	13.572	NaN	25.15892
GIpr05	HEOBI	########	5	11	-50.691	76.18671	27.986	NaN	35.59774
GIpr05	HEOBI	########	5	10	-50.691	76.18671	68.373	NaN	22.25919
GIpr05	HEOBI	########	5	9	-50.691	76.18671	98.086	NaN	20.04955
GIpr05	HEOBI	########	5	8	-50.691	76.18671	147.752	NaN	10.99818
GIpr05	HEOBI	########	5	7	-50.691	76.18671	196.864	NaN	7.585468
GIpr05	HEOBI	########	5	6	-50.691	76.18671	294.875	NaN	2.922109
GIpr05	HEOBI	########	5	5	-50.691	76.18671	690.015	NaN	1.790626
GIpr05	HEOBI	########	5	4	-50.691	76.18671	986.243	NaN	1.253079
GIpr05	HEOBI	########	5	3	-50.691	76.18671	1970.959	NaN	1.333103
GIpr05	HEOBI	########	5	2	-50.691	76.18671	2951.099	NaN	1.633958
GIpr05	HEOBI	########	5	1	-50.691	76.18671	2974.75	NaN	0.252053
GIpr05	HEOBI	########	6	12	-50.7888	75.78225	12.99	NaN	NaN
GIpr05	HEOBI	########	6	11	-50.7888	75.78225	28.012	NaN	NaN
GIpr05	HEOBI	########	6	10	-50.7888	75.78225	67.962	NaN	NaN
GIpr05	HEOBI	########	6	9	-50.7888	75.78225	97.807	NaN	NaN
GIpr05	HEOBI	########	6	8	-50.7888	75.78225	196.296	NaN	NaN
GIpr05	HEOBI	########	6	7	-50.7888	75.78225	294.808	NaN	NaN
GIpr05	HEOBI	########	6	6	-50.7888	75.78225	492.79	NaN	NaN
GIpr05	HEOBI	########	6	5	-50.7888	75.78225	690.474	NaN	NaN
GIpr05	HEOBI	########	6	4	-50.7888	75.78225	986.176	NaN	NaN
GIpr05	HEOBI	########	6	3	-50.7888	75.78225	1479.401	NaN	NaN

GIpr05	HEOBI	########	6	2	-50.7888	75.78225	1577.708	NaN	NaN
GIpr05	HEOBI	########	6	1	-50.7888	75.78225	1627.844	NaN	NaN
GIpr05	HEOBI	########	7	12	-50.8996	75.37746	13.768	NaN	NaN
GIpr05	HEOBI	########	7	11	-50.8996	75.37746	27.59	NaN	NaN
GIpr05	HEOBI	########	7	10	-50.8996	75.37746	67.576	NaN	NaN
GIpr05	HEOBI	########	7	9	-50.8996	75.37746	97.671	NaN	NaN
GIpr05	HEOBI	########	7	8	-50.8996	75.37746	147.009	NaN	NaN
GIpr05	HEOBI	########	7	7	-50.8996	75.37746	197.766	NaN	NaN
GIpr05	HEOBI	########	7	6	-50.8996	75.37746	246.005	NaN	NaN
GIpr05	HEOBI	########	7	5	-50.8996	75.37746	295.014	NaN	NaN
GIpr05	HEOBI	########	7	4	-50.8996	75.37746	345.101	NaN	NaN
GIpr05	HEOBI	########	7	3	-50.8996	75.37746	394.025	NaN	NaN
GIpr05	HEOBI	########	7	2	-50.8996	75.37746	414.187	NaN	NaN
GIpr05	HEOBI	########	7	1	-50.8996	75.37746	434.647	NaN	NaN
GIpr05	HEOBI	########	9	12	-51.2871	73.80983	14.116	NaN	57.85064
GIpr05	HEOBI	########	9	11	-51.2871	73.80983	23.794	NaN	50.71496
GIpr05	HEOBI	########	9	10	-51.2871	73.80983	38.729	NaN	16.72643
GIpr05	HEOBI	########	9	9	-51.2871	73.80983	67.481	NaN	15.7856
GIpr05	HEOBI	########	9	8	-51.2871	73.80983	96.781	NaN	16.74272
GIpr05	HEOBI	########	9	7	-51.2871	73.80983	146.734	NaN	14.39615
GIpr05	HEOBI	########	9	6	-51.2871	73.80983	195.713	NaN	11.57648
GIpr05	HEOBI	########	9	5	-51.2871	73.80983	245.553	NaN	7.712186
GIpr05	HEOBI	########	9	4	-51.2871	73.80983	295.364	NaN	6.42497
GIpr05	HEOBI	########	9	3	-51.2871	73.80983	345.164	NaN	5.673204
GIpr05	HEOBI	########	9	2	-51.2871	73.80983	373.865	NaN	6.234043
GIpr05	HEOBI	########	9	1	-51.2871	73.80983	394.853	NaN	6.83727
GIpr05	HEOBI	########	10	12	-51.5064	72.99996	13.926	NaN	73.57338
GIpr05	HEOBI	########	10	11	-51.5064	72.99996	27.638	NaN	45.6466
GIpr05	HEOBI	########	10	10	-51.5064	72.99996	48.288	NaN	33.8083
GIpr05	HEOBI	########	10	9	-51.5064	72.99996	72.306	NaN	28.22148
GIpr05	HEOBI	########	10	8	-51.5064	72.99996	118.034	NaN	15.29694
GIpr05	HEOBI	########	10	7	-51.5064	72.99996	146.932	NaN	10.52844
GIpr05	HEOBI	########	10	6	-51.5064	72.99996	200.319	NaN	5.792809
GIpr05	HEOBI	########	10	5	-51.5064	72.99996	249.995	NaN	3.52822
GIpr05	HEOBI	########	10	4	-51.5064	72.99996	300.868	NaN	4.624608
GIpr05	HEOBI	########	10	3	-51.5064	72.99996	316.094	NaN	4.71675
GIpr05	HEOBI	########	10	2	-51.5064	72.99996	349.314	NaN	NaN
GIpr05	HEOBI	########	10	1	-51.5064	72.99996	358.374	NaN	3.004176
GIpr05	HEOBI	########	11	12	-52.9275	71.36159	13.106	NaN	30.19517
GIpr05	HEOBI	########	11	11	-52.9275	71.36159	28.641	NaN	33.39405
GIpr05	HEOBI	########	11	10	-52.9275	71.36159	67.823	NaN	32.64753
GIpr05	HEOBI	########	11	9	-52.9275	71.36159	98.108	NaN	17.73527
GIpr05	HEOBI	########	11	8	-52.9275	71.36159	197.196	NaN	6.01594
GIpr05	HEOBI	########	11	7	-52.9275	71.36159	295.385	NaN	2.746298
GIpr05	HEOBI	########	11	6	-52.9275	71.36159	493.073	NaN	1.413807
GIpr05	HEOBI	########	11	5	-52.9275	71.36159	689.369	NaN	1.94688
GIpr05	HEOBI	########	11	4	-52.9275	71.36159	986.512	NaN	1.447222

GIpr05	HEOBI	########	11	3	-52.9275	71.36159	1577.817	NaN	1.453966
GIpr05	HEOBI	########	11	2	-52.9275	71.36159	2559.788	NaN	1.347548
GIpr05	HEOBI	########	11	1	-52.9275	71.36159	2658.453	NaN	1.158779
GIpr05	HEOBI	########	12	6	-53.0323	72.65818	13.138	NaN	NaN
GIpr05	HEOBI	########	12	5	-53.0323	72.65818	28.272	NaN	NaN
GIpr05	HEOBI	########	12	4	-53.0323	72.65818	47.471	NaN	NaN
GIpr05	HEOBI	########	12	3	-53.0323	72.65818	66.55	NaN	NaN
GIpr05	HEOBI	########	12	2	-53.0323	72.65818	87.496	NaN	NaN
GIpr05	HEOBI	########	12	1	-53.0323	72.65818	102.059	NaN	NaN
GIpr05	HEOBI	########	13	10	-52.9988	72.62552	13.573	0.5	30.9583
GIpr05	HEOBI	########	13	9	-52.9988	72.62552	28.897	0.31	20.60596
GIpr05	HEOBI	########	13	8	-52.9988	72.62552	48.619	0.36	20.7981
GIpr05	HEOBI	########	13	7	-52.9988	72.62552	67.37	0.35	19.42686
GIpr05	HEOBI	########	13	6	-52.9988	72.62552	96.928	0.35	21.55899
GIpr05	HEOBI	########	13	2	-52.9988	72.62552	117.577	0.32	20.66585
GIpr05	HEOBI	########	13	1	-52.9988	72.62552	132.135	0.25	19.7409
GIpr05	HEOBI	########	14	7	-53.0351	72.55227	13.189	0.03057	22.7589
GIpr05	HEOBI	########	14	6	-53.0351	72.55227	28.556	0.056044	19.31646
GIpr05	HEOBI	########	14	5	-53.0351	72.55227	47.805	0.101899	17.45076
GIpr05	HEOBI	########	14	4	-53.0351	72.55227	97.631	0.282769	15.14302
GIpr05	HEOBI	########	14	3	-53.0351	72.55227	122.492	0.229272	16.82578
GIpr05	HEOBI	########	14	2	-53.0351	72.55227	157.154	0.315886	16.06095
GIpr05	HEOBI	########	14	1	-53.0351	72.55227	172.227	0.254746	14.83105
GIpr05	HEOBI	########	15	6	-53.0726	72.5929	13.53	0.427981	25.73479
GIpr05	HEOBI	########	15	5	-53.0726	72.5929	28.565	0.537465	24.82952
GIpr05	HEOBI	########	15	4	-53.0726	72.5929	48.532	0.547418	24.93982
GIpr05	HEOBI	########	15	3	-53.0726	72.5929	68.211	0.497653	21.98645
GIpr05	HEOBI	########	15	2	-53.0726	72.5929	98.274	0.338404	24.81739
GIpr05	HEOBI	########	15	1	-53.0726	72.5929	117.496	0.517559	23.09538
GIpr05	HEOBI	########	16	6	-52.9846	72.55511	13.3	0.128819	35.1506
GIpr05	HEOBI	########	16	5	-52.9846	72.55511	28.356	0.110417	33.03102
GIpr05	HEOBI	########	16	4	-52.9846	72.55511	67.882	0.184028	29.02345
GIpr05	HEOBI	########	16	3	-52.9846	72.55511	121.723	0.220833	25.11476
GIpr05	HEOBI	########	16	2	-52.9846	72.55511	175.822	0.257639	18.38147
GIpr05	HEOBI	########	16	1	-52.9846	72.55511	187.19	0.147222	0
GIpr05	HEOBI	########	18	12	-54.1674	73.66494	12.621	-3.43E-17	34.94551
GIpr05	HEOBI	########	18	11	-54.1674	73.66494	27.79	0.042798	33.83229
GIpr05	HEOBI	########	18	10	-54.1674	73.66494	67.787	0.027984	32.01916
GIpr05	HEOBI	########	18	9	-54.1674	73.66494	96.889	0.054321	21.55846
GIpr05	HEOBI	########	18	8	-54.1674	73.66494	147.647	0.097119	4.046461
GIpr05	HEOBI	########	18	7	-54.1674	73.66494	197.004	0.098765	7.756472
GIpr05	HEOBI	########	18	6	-54.1674	73.66494	294.459	0.083951	2.209019
GIpr05	HEOBI	########	18	5	-54.1674	73.66494	491.785	0.077366	2.004212
GIpr05	HEOBI	########	18	4	-54.1674	73.66494	690.635	-0.01152	1.602537
GIpr05	HEOBI	########	18	3	-54.1674	73.66494	987.414	0.014815	1.8537
GIpr05	HEOBI	########	19	6	-53.0599	73.98966	13.634	0.230366	29.34913
GIpr05	HEOBI	########	19	5	-53.0599	73.98966	28.061	0.307155	26.43874

GIpr05	HEOBI	########	19	4	-53.0599	73.98966	48.381	0.244328	27.07139
GIpr05	HEOBI	########	19	3	-53.0599	73.98966	68.133	0.272251	26.25336
GIpr05	HEOBI	########	19	2	-53.0599	73.98966	78.164	0.230366	28.38649
GIpr05	HEOBI	########	19	1	-53.0599	73.98966	88.034	0.237347	28.59244
GIpr05	HEOBI	########	20	6	-53.2133	73.63984	13.756	0.293194	33.14566
GIpr05	HEOBI	########	20	5	-53.2133	73.63984	28.439	0.321117	32.40409
GIpr05	HEOBI	########	20	4	-53.2133	73.63984	47.896	0.223386	27.98615
GIpr05	HEOBI	########	20	3	-53.2133	73.63984	67.178	0.244328	29.29488
GIpr05	HEOBI	########	20	2	-53.2133	73.63984	88.051	0.268761	27.47886
GIpr05	HEOBI	########	20	1	-53.2133	73.63984	93.088	0.279232	26.53593
GIpr05	HEOBI	########	21	8	-53.2808	73.31556	13.271	0.024931	37.01473
GIpr05	HEOBI	########	21	7	-53.2808	73.31556	28.651	0.124098	34.44433
GIpr05	HEOBI	########	21	6	-53.2808	73.31556	48.765	0.215488	22.88427
GIpr05	HEOBI	########	21	5	-53.2808	73.31556	68.321	0.074794	14.49503
GIpr05	HEOBI	########	21	4	-53.2808	73.31556	88.306	0.093742	12.79084
GIpr05	HEOBI	########	21	3	-53.2808	73.31556	98.136	0.130142	13.49046
GIpr05	HEOBI	########	21	2	-53.2808	73.31556	107.543	0.06183	23.37634
GIpr05	HEOBI	########	21	1	-53.2808	73.31556	112.6	0.218399	16.53867
GIpr05	HEOBI	########	22	6	-52.9604	73.23888	13.757	0.438672	25.29686
GIpr05	HEOBI	########	22	5	-52.9604	73.23888	27.955	0.415584	25.80142
GIpr05	HEOBI	########	22	4	-52.9604	73.23888	49.145	0.325156	26.9169
GIpr05	HEOBI	########	22	3	-52.9604	73.23888	68.045	0.2886	21.43639
GIpr05	HEOBI	########	22	2	-52.9604	73.23888	86.872	0.305916	20.9332
GIpr05	HEOBI	########	22	1	-52.9604	73.23888	108.445	0.323232	20.60044
GIpr05	HEOBI	########	23	6	-53.0059	73.72118	14.402	0.498551	24.04201
GIpr05	HEOBI	########	23	5	-53.0059	73.72118	28.24	0.510145	27.07191
GIpr05	HEOBI	########	23	4	-53.0059	73.72118	48.053	0.307246	27.38061
GIpr05	HEOBI	########	23	3	-53.0059	73.72118	59.322	0.301449	24.98825
GIpr05	HEOBI	########	23	2	-53.0059	73.72118	67.7	0.26087	23.05525
GIpr05	HEOBI	########	23	1	-53.0059	73.72118	75.02	0.272464	25.44332
GIpr05	HEOBI	########	24	4	-53.0037	73.60683	13.901	0.473491	27.52554
GIpr05	HEOBI	########	24	3	-53.0037	73.60683	20.519	0.537533	29.27902
GIpr05	HEOBI	########	24	2	-53.0037	73.60683	28.885	0.538583	28.27456
GIpr05	HEOBI	########	24	1	-53.0037	73.60683	35.27	0.571129	27.81576
GIpr05	HEOBI	########	25	6	-53.035	72.66254	13.872	0.283465	13.54655
GIpr05	HEOBI	########	25	5	-53.035	72.66254	29.071	0.272966	13.22903
GIpr05	HEOBI	########	25	4	-53.035	72.66254	58.134	0.356955	14.14021
GIpr05	HEOBI	########	25	3	-53.035	72.66254	87.731	0.39895	16.02761
GIpr05	HEOBI	########	25	2	-53.035	72.66254	108.245	0.39895	27.36035
GIpr05	HEOBI	########	25	1	-53.035	72.66254	119.586	0.388451	31.96008
GIpr05	HEOBI	########	26	6	-53.0288	72.66081	12.864	0.427142	17.44573
GIpr05	HEOBI	########	26	5	-53.0288	72.66081	28.669	0.308532	19.442
GIpr05	HEOBI	########	26	4	-53.0288	72.66081	58.001	0.349281	20.15696
GIpr05	HEOBI	########	26	3	-53.0288	72.66081	88.469	0.390031	23.70023
GIpr05	HEOBI	########	26	2	-53.0288	72.66081	107.496	0.336183	15.88943
GIpr05	HEOBI	########	26	1	-53.0288	72.66081	119.969	0.38421	23.84019
GIpr05	HEOBI	########	27	6	-53.0334	72.66873	13.921	0.302711	23.04924

GIpr05	HEOBI	########	27	5	-53.0334	72.66873	28.669	0.350737	23.0427
GIpr05	HEOBI	########	27	4	-53.0334	72.66873	58.347	0.437329	24.48343
GIpr05	HEOBI	########	27	3	-53.0334	72.66873	88.273	0.458432	26.38703
GIpr05	HEOBI	########	27	2	-53.0334	72.66873	107.923	0.448972	29.35477
GIpr05	HEOBI	########	27	1	-53.0334	72.66873	119.736	0.439512	27.47414
GIpr05	HEOBI	########	28	6	-53.0387	72.66159	12.73	0.346371	23.04924
GIpr05	HEOBI	########	28	5	-53.0387	72.66159	28.458	0.628707	23.0427
GIpr05	HEOBI	########	28	4	-53.0387	72.66159	58.665	0.311543	24.48343
GIpr05	HEOBI	########	28	3	-53.0387	72.66159	88.021	0.377837	26.38703
GIpr05	HEOBI	########	28	2	-53.0387	72.66159	107.833	0.655835	30.31347
GIpr05	HEOBI	########	28	1	-53.0387	72.66159	117.306	0.420439	27.87476
GIpr05	HEOBI	########	29	6	-53.0337	72.65347	13.39	0.352406	28.24213
GIpr05	HEOBI	########	29	5	-53.0337	72.65347	28.975	0.453477	28.03404
GIpr05	HEOBI	########	29	4	-53.0337	72.65347	56.947	1.014404	25.67791
GIpr05	HEOBI	########	29	3	-53.0337	72.65347	78.064	0.507424	30.14941
GIpr05	HEOBI	########	29	2	-53.0337	72.65347	92.863	0.490539	24.73785
GIpr05	HEOBI	########	29	1	-53.0337	72.65347	101.019	0.472865	29.28149
GIpr05	HEOBI	########	30	6	-52.922	74.02227	13.878	5.173907	43.38744
GIpr05	HEOBI	########	30	5	-52.922	74.02227	28.235	0.285676	41.37166
GIpr05	HEOBI	########	30	4	-52.922	74.02227	67.518	0.126967	42.97981
GIpr05	HEOBI	########	30	3	-52.922	74.02227	98.262	0.158709	39.67458
GIpr05	HEOBI	########	30	2	-52.922	74.02227	147.422	0.142838	38.21724
GIpr05	HEOBI	########	30	1	-52.922	74.02227	186.937	0.190451	25.03412
GIpr05	HEOBI	########	31	9	-52.6964	74.79167	12.603	-0.00447	59.0513
GIpr05	HEOBI	########	31	8	-52.6964	74.79167	48.258	5.418345	57.53533
GIpr05	HEOBI	########	31	7	-52.6964	74.79167	97.416	0.214765	40.96099
GIpr05	HEOBI	########	31	6	-52.6964	74.79167	147.418	0.035794	23.17195
GIpr05	HEOBI	########	31	5	-52.6964	74.79167	245.205	0.102908	21.56045
GIpr05	HEOBI	########	31	4	-52.6964	74.79167	345.04	0.06264	21.72319
GIpr05	HEOBI	########	31	3	-52.6964	74.79167	395.434	0.008949	15.81971
GIpr05	HEOBI	########	31	2	-52.6964	74.79167	443.703	0.008949	11.57393
GIpr05	HEOBI	########	31	1	-52.6964	74.79167	468.562	0.040268	11.38487
GIpr05	HEOBI	########	32	6	-52.5428	75.26237	12.871	0.014625	52.81464
GIpr05	HEOBI	########	32	5	-52.5428	75.26237	47.889	0.102377	53.72495
GIpr05	HEOBI	########	32	4	-52.5428	75.26237	87.467	0.146252	27.12847
GIpr05	HEOBI	########	32	3	-52.5428	75.26237	147.438	0.204753	17.14814
GIpr05	HEOBI	########	32	2	-52.5428	75.26237	196.365	0.146252	18.88747
GIpr05	HEOBI	########	32	1	-52.5428	75.26237	271.03	0.043876	15.17406
GIpr05	HEOBI	########	33	9	-52.4092	75.60666	14.22	0	50.26546
GIpr05	HEOBI	########	33	8	-52.4092	75.60666	48.259	0.131627	46.00405
GIpr05	HEOBI	########	33	7	-52.4092	75.60666	97.726	0	26.69294
GIpr05	HEOBI	########	33	6	-52.4092	75.60666	148.04	0.058501	15.31341
GIpr05	HEOBI	########	33	5	-52.4092	75.60666	221.234	0.087751	13.07136
GIpr05	HEOBI	########	33	4	-52.4092	75.60666	293.952	0.190128	10.73295
GIpr05	HEOBI	########	33	3	-52.4092	75.60666	394.851	0.014625	8.649526
GIpr05	HEOBI	########	33	2	-52.4092	75.60666	494.551	0.014625	7.107548
GIpr05	HEOBI	########	33	1	-52.4092	75.60666	526.794	0.02925	7.067597

GIpr05	HEOBI	########	34	9	-52.302	76.00671	13.47	0.301075	51.48856
GIpr05	HEOBI	########	34	8	-52.302	76.00671	48.05	0	49.68593
GIpr05	HEOBI	########	34	7	-52.302	76.00671	96.09	0	46.84237
GIpr05	HEOBI	########	34	6	-52.302	76.00671	147.486	0.064516	14.18614
GIpr05	HEOBI	########	34	5	-52.302	76.00671	219.642	0.086022	11.46784
GIpr05	HEOBI	########	34	4	-52.302	76.00671	296.809	0.150538	7.291876
GIpr05	HEOBI	########	34	3	-52.302	76.00671	444.724	0.086022	5.358688
GIpr05	HEOBI	########	34	2	-52.302	76.00671	542.576	0.064516	7.641063
GIpr05	HEOBI	########	35	6	-52.8381	74.32217	13.648	0.053872	36.59579
GIpr05	HEOBI	########	35	5	-52.8381	74.32217	28.746	0.094276	36.38404
GIpr05	HEOBI	########	35	4	-52.8381	74.32217	68.064	0.13468	24.47819
GIpr05	HEOBI	########	35	3	-52.8381	74.32217	97.401	0.074074	13.58863
GIpr05	HEOBI	########	35	2	-52.8381	74.32217	137.334	0.141414	14.78911
GIpr05	HEOBI	########	35	1	-52.8381	74.32217	146.741	0.074074	12.68924
GIpr05	HEOBI	########	36	4	-53.0077	73.70902	14.094	0.13001	23.77608
GIpr05	HEOBI	########	36	3	-53.0077	73.70902	28.533	0.210981	19.01267
GIpr05	HEOBI	########	36	2	-53.0077	73.70902	58.272	0.171065	16.10411
GIpr05	HEOBI	########	36	1	-53.0077	73.70902	71.277	0.222059	23.41104
GIpr05	HEOBI	########	37	4	-53.0118	73.71645	13.71	0.23165	22.28596
GIpr05	HEOBI	########	37	3	-53.0118	73.71645	28.479	0.179125	23.42051
GIpr05	HEOBI	########	37	2	-53.0118	73.71645	58.461	0.183165	24.30983
GIpr05	HEOBI	########	37	1	-53.0118	73.71645	68.211	0.167003	23.10616
GIpr05	HEOBI	########	38	4	-53.0074	73.72444	14.088	-0.00458	22.98903
GIpr05	HEOBI	########	38	3	-53.0074	73.72444	28.569	0.280673	23.51511
GIpr05	HEOBI	########	38	2	-53.0074	73.72444	58.511	0.320269	24.6925
GIpr05	HEOBI	########	38	1	-53.0074	73.72444	75.355	0.036633	21.34652
GIpr05	HEOBI	########	39	4	-53.0027	73.71675	13.46	0.136835	20.77638
GIpr05	HEOBI	########	39	3	-53.0027	73.71675	28.716	0.193346	22.57333
GIpr05	HEOBI	########	39	2	-53.0027	73.71675	45.62	0.122696	21.4729
GIpr05	HEOBI	########	39	1	-53.0027	73.71675	77.198	0.330879	19.88652
GIpr05	HEOBI	########	40	5	-53.0076	73.7161	13.771	0.059379	23.32216
GIpr05	HEOBI	########	40	4	-53.0076	73.7161	28.819	0.043185	20.80127
GIpr05	HEOBI	########	40	3	-53.0076	73.7161	48.649	0.059379	22.35696
GIpr05	HEOBI	########	40	2	-53.0076	73.7161	63.429	0.010796	21.3951
GIpr05	HEOBI	########	40	1	-53.0076	73.7161	72.432	0.002699	21.16987

ONC_BOTTLE